



ORIGINAL ARTICLE

Novel benzimidazole derivatives as anti-cervical cancer agents of potential multi-targeting kinase inhibitory activity



Eman A. Abd El-Meguid^{a,*}, Eman M. Mohi El-Deen^b, Manal A. Nael^c,
Manal M. Anwar^b

^a Department of Chemistry of Natural and Microbial Products, Pharmaceutical and Drug Industries Research Division, National Research Centre, Dokki, Cairo 12622, Egypt

^b Department of Therapeutic Chemistry, Pharmaceutical and Drug Industries Research Division, National Research Centre, Dokki, Cairo 12622, Egypt

^c Department of Pharmaceutical Chemistry, Faculty of Pharmacy, Tanta University, Tanta 31527, Egypt

Received 4 September 2020; accepted 29 October 2020

Available online 6 November 2020

KEYWORDS

6-Benzoylbenzimidazole;
Cervical cancer;
EGFR;
HER2;
Apoptosis;
Molecular docking

Abstract Multi-target EGFR, HER2, VEGFR-2 and PDGFR is an improved strategy for the treatment of solid tumors. This work deals with synthesis of an array of new 6-benzoyl benzimidazole derivatives utilizing 1-(6-benzoyl-2-(3,4-dimethoxyphenyl)-1H benzo[d]imidazol-1-yl)propan-2-one (**1**) as a starting compound. The new compounds were screened as cytotoxic agents against cervical cancer cells (Hela) and Doxorubicin served as a reference drug. Most of the tested compounds showed promising anticancer activity in addition to their safety towards the normal cell line. The most potent candidates were evaluated as EGFR, HER2, PDGFR- β and VEGFR2 inhibitors in comparison to Erlotinib. Compounds **9** and **13** exhibited promising suppression effects. Also, the latter compounds exhibited their ability to induce cellular apoptosis alongside cell cycle arrest at the G2/M phase and accumulation of cells in pre-G1 phase. Molecular docking analysis suggested that compounds **2c**, **3f**, **9**, **12** and **13** tightly interacts with the amino acid residues in the active binding site of HER2 kinase.

© 2020 The Authors. Published by Elsevier B.V. on behalf of King Saud University. This is an open access article under the CC BY-NC-ND license (<http://creativecommons.org/licenses/by-nc-nd/4.0/>).

1. Introduction

Cervical cancer disease is assumed to be the fourth most common cancer affecting women worldwide. It has been estimated about 570 000 cases and 311 000 deaths in 2018, accounting for 3.3% of all cancer-related deaths (Vora and Gupta, 2018; Abbas, and Abd El-Karim, 2019). Metastasis develops in 15% to 61% of women with cervical cancer within the first

* Corresponding author.

E-mail address: ea.mabrouk@nrc.sci.eg (Eman A. Abd El-Meguid).

Peer review under responsibility of King Saud University.



Production and hosting by Elsevier

2 years of completing treatment (Šarenac and Mikov, 2019; Ueda et al., 2017). Cervical cancer has moderate to high levels of epidermal growth factor receptor (EGFR) protein expression. The percentage of cervical adenocarcinoma cases in which EGFR expression was detected varied from 19% to 67% in previous studies, and its overexpression was shown to be associated with poor prognosis (Pérez-Regadera et al., 2011). As single agents in the treatment of recurrent cervical cancer, Gefitinib and Erlotinib have shown minimal activity (Schilder et al., 2009; Goncalves et al., 2008).

The human epidermal growth factor receptor (HER) family is categorized into four candidates, which are HER1 (EGFR/ ErbB1), HER2 (ErbB2/neu), HER3 (ErbB3) and HER4 (ErbB4) that are only expressed at low levels in normal human tissues (Soliman et al., 2019; Hou et al., 2019).

It has been reported that, several malignant tumors including breast, cervix, ovary, lung, colon, head, and neck are associated with deregulation of HER family signaling enhancing proliferation, invasion, metastasis, angiogenesis, and tumor cell survival (Zou et al., 2018). Additionally, the up regulation of EGFR and HER2 receptors is correlated with therapeutic resistance, which represents a significant rationale for continuous urgent need for drug intervention (El-Sherief et al., 2018).

Molecular targeted medications represent one of the main strategies in the research of novel cancer targets and associated pathways (Oh et al., 2015). Many EGFR and HER2 targeted drugs were approved by the U.S. Food and Drug Administration (FDA) in recent years. They are currently divided into (i) first generation drugs that interact reversibly to EGFR (such as; Gefitinib, Erlotinib, Icotinib and Lapatinib), (ii) second generation drugs of irreversible dual EGFR/HER2 binding thereby, enhancing their potencies by suppressing EGFR signaling more effectively (such as Afatinib, Dacomitinib and Neratinib) and (iii) third-generation agents that overcome resistance to the previous two generations (such as; Nazartinib, Avitinib and Osimertinib) (Das et al., 2019; Kujtan and Subramanian, 2019) (Fig. 1).

Benzimidazole is an isostere of purine nucleosides so; it is widely used as a basic nucleus in the development of different anticancer agents (Jawaid Akhtar et al., 2018; Shrivastava et al., 2017). Various researches investigated that benzimidazole derivatives showing anticancer properties introduce their activities through different mechanisms *via* DNA intercalation, topoisomerases-I & II inhibition, androgen receptor antagonistic effect, poly (ADP-ribose) polymerase (PARP), dihydrofolate reductase (DHFR) enzymes and microtubule inhibiting activity. Moreover, different anticancer benzimidazole candidates were confirmed as potent EGFR inhibitors (Shrivastava et al., 2017). In addition, the third generation EGFR inhibitor Nazartinib has a benzimidazole structure and the other two candidates Avitinib and Osimertinib (Zhang, 2016) are indolopyrimidine and indole derivatives, which are bio-isosteres to benzimidazole ring.

Recently, a paradigm change have been confirmed in designing the significant selective agents targeting a single protein or gene to controlling a multiplicity of targets within related signaling pathways (Elzahhar et al., 2019). Hence, this effort was focused on seeking for new multi-targeting anti-cervical cancer leads of high activity and selectivity with low toxicity that can be reached to the clinical stages.

In continuation of our previous efforts to gain new compounds bearing various heterocyclic scaffolds of efficient anticancer activity targeting different enzymes (Abd El-Meguid et al., 2019; Abd El-Meguid, and Ali, 2016), in this work, Nazartinib structure helped for rational design and synthesis of new derivatives bearing 6-benzoyl benzimidazole scaffold hybridized at C-2 with 3,4-dimethoxyphenyl moiety and at position N-1 with substituted phenylbut-3-en-2-one **I**, substituted phenyl iminopropyl **II**, propan-2-ylidene-hydrazine-1-(*t* hio)carboxamide side chains **III** and propan-2-ylidenehydrazine-thiazoline/thiazolidin-4-one side chain **IV** (Fig. 2). The newly prepared compounds were evaluated as anti-cervical cancer agents. Furthermore, the most active derivatives were evaluated as EGFR/HER2 inhibitors. Additionally, the most promising derivatives were further subjected to kinase inhibition assay against the other two receptor tyrosine kinases (RTKs); vascular endothelial growth factor receptor-2 (VEGFR-2) and platelet-derived growth factor receptor (PDGFR- β) as well as cell cycle analysis and apoptosis induction study. Molecular docking study was performed for the most promising structures inside the active site of HER2 to confirm their possible mechanism of action.

2. Result and discussion

2.1. Synthesis

The synthetic approaches of the targeted benzimidazole compounds were described in Schemes 1-3. The key starting compound 1-(6-benzoyl-2-(3,4-dimethoxyphenyl)-1*H*-benzo[*d*]imidazol-1-yl)propan-2-one (**1**) was prepared by the reaction of *o*-phenylenediamine **A** with 3,4-dimethoxybenzaldehyde to give the corresponding (2-(3,4-dimethoxyphenyl)-1*H*-benzo[*d*]imidazol-6-yl)(phenyl)methanone derivative **B** which was alkylated with chloroacetone in dry acetone in the presence of potassium carbonate as a basic medium to give the target starting precursor **1**. Compound **1** was allowed to react with different appropriate aromatic aldehydes in ethyl alcohol in the presence of a catalytic amount of piperidine as a basic medium to give the corresponding chalcone derivatives **2a-2e**. In order to construct the Schiff bases **3a-3f**, the starting **1** was heated with various aromatic amines in ethanol containing a few amounts of acetic acid at the refluxing temperature (Scheme 1).

Also, compound **1** was allowed to react with hydrazine hydrate in absolute ethanol to give the corresponding hydrazone derivative **4**, while its reaction with *p*-toluic hydrazide and 2-furoic acid hydrazide led to the formation of the corresponding hydrazone derivatives **5** and **6** (Scheme 2). When the acetyl compound **1** was condensed with semicarbazide hydrochloride in absolute ethanol in the presence of sodium acetate afforded the corresponding semicarbazone derivative **7**, while condensation of **1** with thiosemicarbazide in ethanol containing a few drops of concentrated hydrochloric acid furnished the corresponding thiosemicarbazone derivative **8**.

The thiosemicarbazone analogue **8** was utilized as a useful intermediate for further preparation of different benzimidazole-heterocyclic compounds. Thus, condensation of **8** with different acid anhydrides such as succinic acid anhydride, maleic acid anhydride and phthalic acid anhydride in acetic acid led to the formation of 2,5-dioxopyrrolidine, 2,5-dioxopyrroline and 1,3-dioxoisindoline derivatives **9**, **10** and

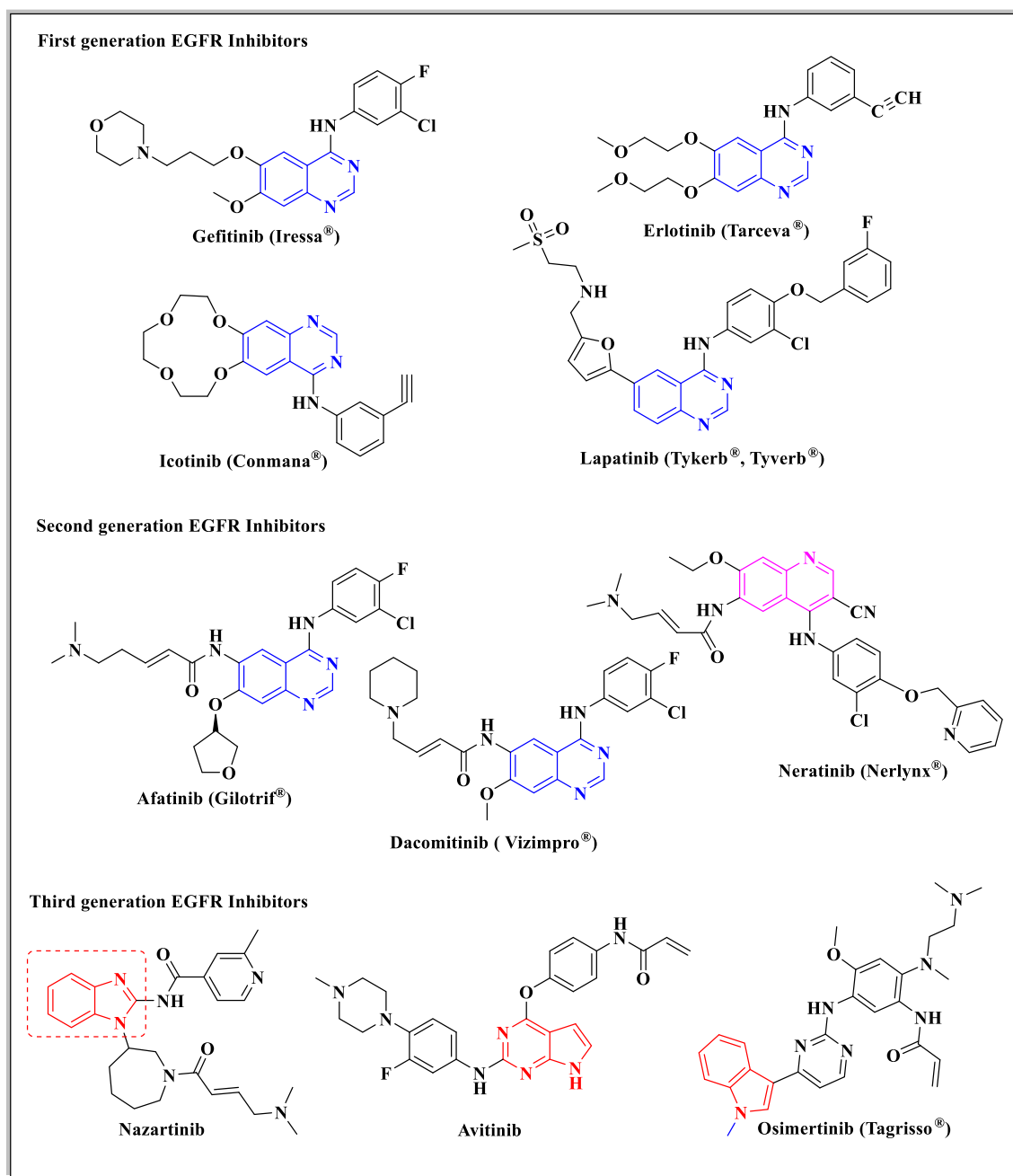


Fig. 1 Various approved drugs of EGFR tyrosine kinase inhibiting activity.

11, respectively. Also, cyclization of the 8 with haloketones such as chloroacetone and ethyl bromoacetate accomplished the thiazoline and thiazolidinone derivatives 12 and 13, respectively (Scheme 3).

2.2. In vitro anticancer activity

The present investigation deals with construction of new derivatives bearing 2-(3,4-dimethoxyphenyl)-1-substituted-benzimidazole scaffold 2–13 for anti-cervical cancer evaluation. Accordingly, the new derivatives were subjected to MTT assay against Hela cell line using Doxorubicin as a reference drug (Thavamani et al., 2013;

Prasetyaningrum et al., 2018) as represented in Fig. 3. The results were tabulated in Table 1. It has been detected that the 4-(dimethylamino)phenylbut-3-en-2-one derivative 2c, the thiazolylsulfonyl derivative 3f, the 2,5-dioxypyrrolidine derivative 9, the 4-methylthiazoline derivative 12 and thiazolidin-4-one 13 exhibited the most potent cytotoxic activity that was higher than that gained by the reference drug (IC_{50} 2c: 1.84, IC_{50} 3f: 1.91; IC_{50} 9: 1.62; IC_{50} 12: 1.71; IC_{50} 13: 1.44; IC_{50} Dox: 2.05 μ M). A slight decrease in the potency was detected by the 4-nitrophenyl-iminopropyl derivative 3c of IC_{50} 3.04 μ M. It could be noted that the increase in the number of nitrogen atoms in addition to the incorporation of thiazole rings or pyrrolidine moiety contributed to more cytotoxic

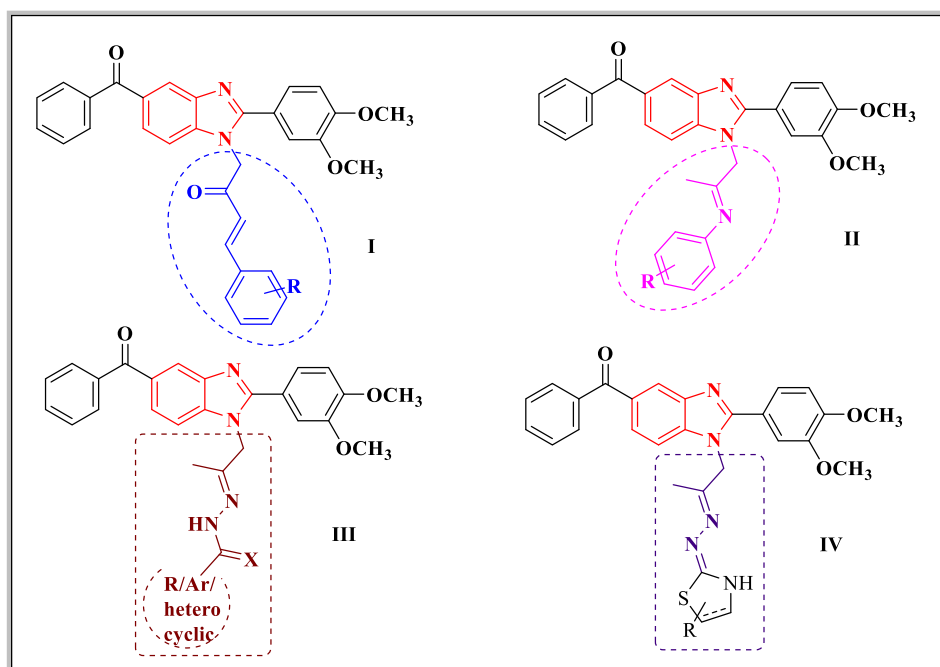


Fig. 2 Newly designed benzimidazole derivatives as EGFR tyrosine kinase inhibitors.

potency. This result comes in agreement with many researches which investigated the unique anticancer activity of different clinically applied anticancer drugs and compounds bearing thiazole and pyrrolidine scaffolds (Sharma et al., 2020; Smolobochkin, et al., 2019). A detectable drop-in the cytotoxic activity of the rest of the compounds was observed inducing IC_{50} values ranging from 6.20 – 28.12 μM . One of the most important drawbacks of the anticancer drugs is the deterioration of the normal cells. Accordingly, the cytotoxic activity of the potent tested compounds (**2c**, **3f**, **9**, **12** and **13**) against cervical cancer cell (Hela) was also examined against the human normal fibroblast cells (WI-38) using Doxorubicin as a reference drug, and their IC_{50} values were determined by the MTT assay. The IC_{50} doses of all tested compounds against the normal cells were higher than their IC_{50} values against the Hela cells (Table 1). The most potent cytotoxic candidates **9** and **13** exhibited significant cytotoxic activity against Hela cell line and noteworthy safety profile against the normal cells.

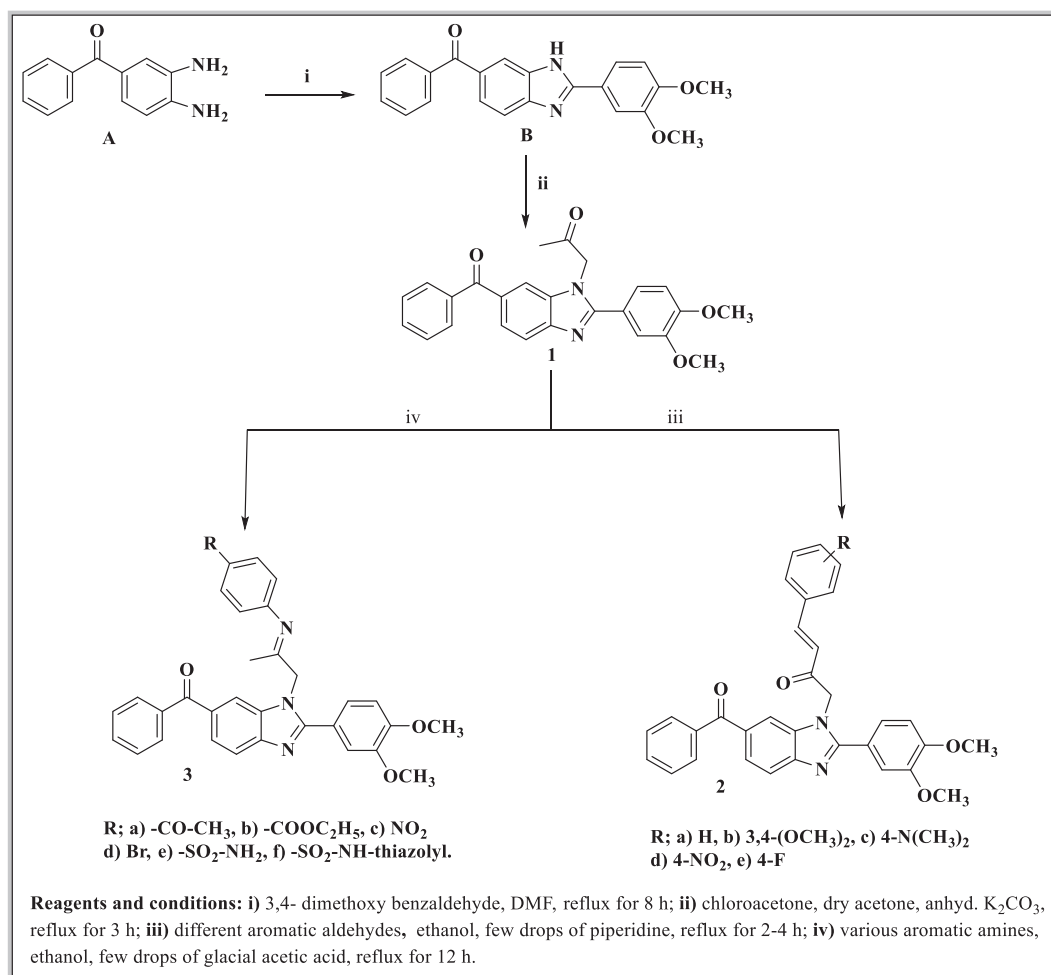
2.3. Evaluation of EGFR/HER2 inhibitory activity

The compounds showing promising cytotoxic potency **2c**, **3f**, **9**, **12** and **13** were further evaluated for their dual EGFR/HER2 inhibitory activity referring to Erlotinib (Table 2, Fig. 4). The 2,5-dioxypyrrolidine derivative **9** and the thiazolidin-4-one **13** represented the most promising potential EGFR inhibiting activity but slightly less than that of the reference Erlotinib (IC_{50} **9**; 0.157, IC_{50} **13**; 0.109 μM , IC_{50} Erlotinib; 0.079 μM) and are more potent than that of the reference Nazartinib (IC_{50} Nazartinib; 0.16 μM). Further decrease in the suppression effect was investigated by the compounds **2c**, **3f** and **12** of IC_{50} values; 0.214, 0.342, 0.305 μM , respectively, which might be contributed to improper fitting in the EGFR active site. On the other hand, all of the examined compounds exhibited significant inhibition against HER2 enzyme. Com-

pound **13** produced 6.5 folds more potency than Erlotinib producing IC_{50} ; 0.19 μM , IC_{50} Erlotinib; 1.23 μM . Furthermore, compound **9** represented 5 folds more inhibition potency of HER2 than the reference drug of IC_{50} ; 0.25 μM . Compounds **12**, **3f** and **2c** were more potent suppressors against HER2 than Erlotinib by 5–3 folds, respectively. Scrutinizing the resultant data, the examined benzimidazole derivatives are more selective towards HER2 than EGFR enzyme and the most potent cytotoxic candidates **9** and **13** induced dual EGFR/HER2 inhibitory activity.

2.4. In vitro kinase inhibition assay

Since it has been reported that the receptor tyrosine kinases (RTKs); EGFR, vascular endothelial growth factor receptor-2 (VEGFR-2) and platelet-derived growth factor receptor (PDGFR) participate significantly in regulating tumor cell proliferation, differentiation, survival, angiogenesis and apoptosis, they were successfully considered as attractive targets for anticancer therapies, particularly for producing multi-target anticancer drugs of improved therapeutic effectiveness (Li et al., 2011; Knight et al., 2010). Additionally, they also work in a synergistic pattern in regulating tumor response to anticancer RTK inhibitor drugs. Hence, multi-target RTK drugs that simultaneously inhibit EGFR, VEGFR-2 and PDGFR- β give substantially optimized anticancer therapeutic effect than drugs that inhibit individual RTKs (Wang et al., 2019). Accordingly, the promising cytotoxic compounds **2c**, **3f**, **9**, **12** and **13** were subjected to kinase assay against PDGFR- β and VEGFR-2. As shown in Table 2, both compounds **9** and **13** exhibited promising inhibitory activity against both kinases (Fig. 5). Interestingly, the thiazoline compound **13** appeared about 3.8 times more potent than the reference drug Erlotinib against PDGFR- β (IC_{50} ; 21.61 μM , IC_{50} Erlotinib; 83.11 μM) and about 1.8 times more potent than Erlotinib



Scheme 1 Synthesis of phenylbuten-2-one-benzimidazole and substituted phenyl iminopropyl – benzimidazole derivatives (**2a-e** and **3a-f**).

against VEGFR-2 (IC_{50} ; 69.62 μM , IC_{50} Erlotinib; 124.7 μM). Furthermore, the 2,5-dioxypyrrolidine derivative **9** showed good inhibitory activities against PDGFR- β (IC_{50} ; 76.09 μM , IC_{50} Erlotinib; 83.11 μM) and against VEGFR-2 (IC_{50} ; 123.27 μM , IC_{50} Erlotinib; 124.7 μM). Further decrease in the suppression effects were investigated by the compounds **2c**, **3f** and **12** of IC_{50} values against PDGFR- β ; 95.31, 89.11, 85.11 μM , respectively, and IC_{50} values against VEGFR-2; 143.44, 138.15, 133.54 μM , respectively.

It could be noted that the potent anti-cancer activity of compound **13** against Hela cells comes as a companion to its significant multi-kinase suppression activity against the receptor tyrosine kinases (RTKs); EGFR, HER-2, PDGFR- β and VEGFR-2.

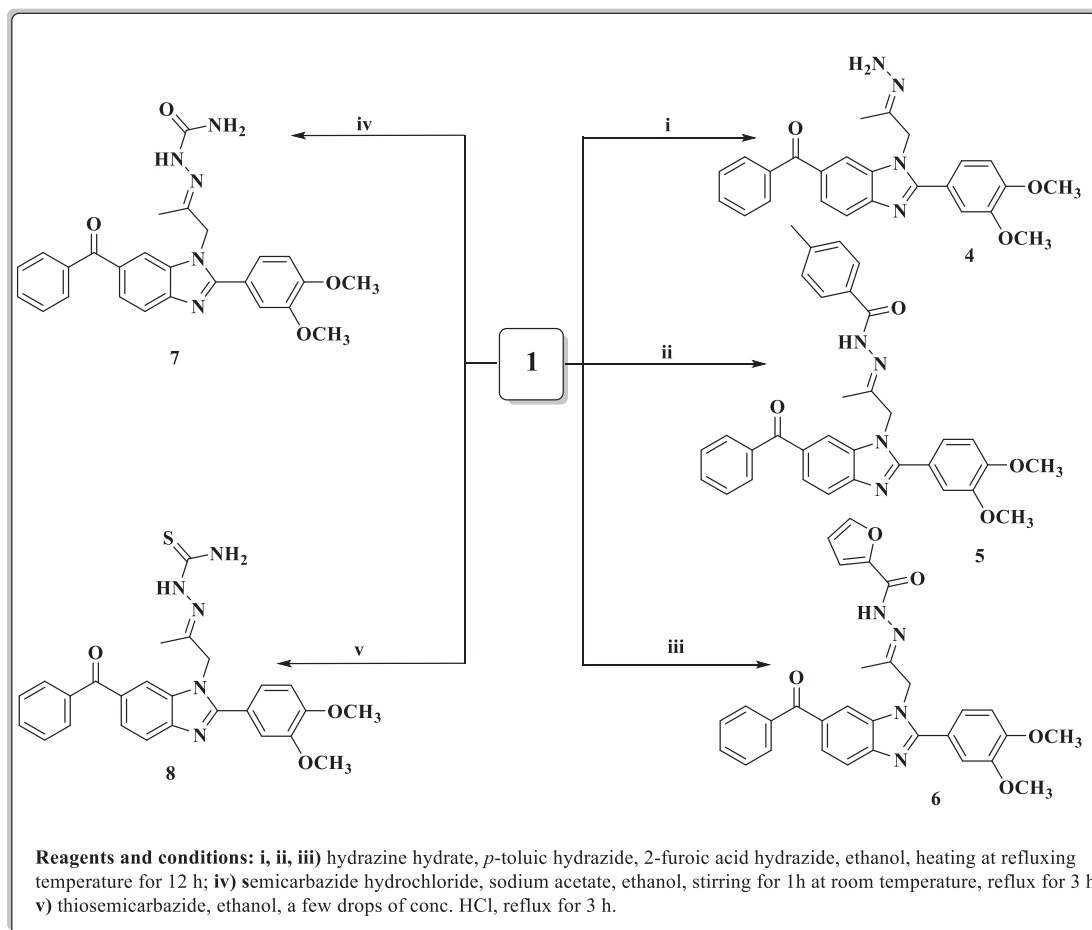
2.5. Cell cycle analysis and detection of apoptosis

The most promising compounds **9** and **13** were selected for further investigation to demonstrate their effects on the progression of cell cycle and apoptosis induction in Hela cell line. Exposure of Hela cells to both compounds **9** and **13** at their IC_{50} concentrations 1.62 and 1.44 μM for 24 h alongside induction of apoptosis were examined. Cells Exposure to both

compounds led an interference with the normal cell cycle distribution. Both compounds **9** and **13** produced a pronounced increment in the cell percentages at pre-G1 phase by 13 and 27 folds, respectively and at G2/M phase by 7 and 10 folds, respectively compared to the untreated Hela cells (Table 3 and Fig. 6). Cumulation of cells in pre-G1 phase might be contributed to degradation of the genetic materials indicating a probable role the tested derivatives in inducing apoptosis in the cancer cells. Furthermore, cumulation of the cells at G2/M phase indicted cell cycle disruption at this stage preventing its mitotic stage.

2.6. Apoptosis detection by annexin V-FITC assay

Apoptosis occurs due to the autonomous and organized destruction of genes-controlled cells (He et al., 2009). In addition, multiple external factors influence its startup. Thus, it was of interest to investigate the relationship between apoptosis of Hela cells and the compounds **9** and **13**. The induction of apoptosis of the latter compounds was examined utilizing annexin V-FITC and propidium iodide (PI) double staining flow cytometry analysis (Cao et al., 2020; Yang et al., 2020). Based on the obtained results presented in Table 4 and



Scheme 2 Synthesis of hydrazine-(thio)carboxamide-benzimidazole derivatives (4-8).

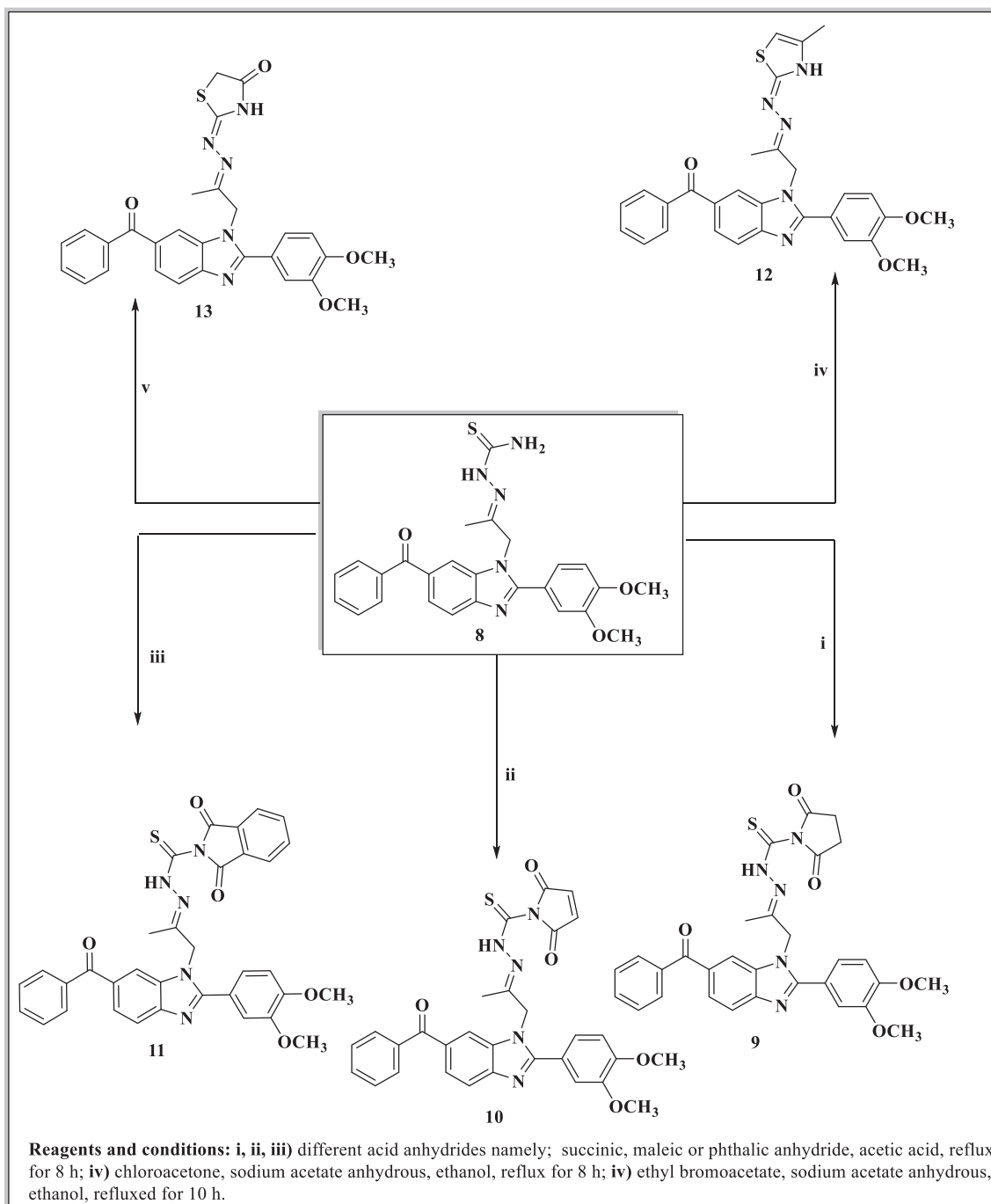
Fig. 7, both derivatives effectively induced cell apoptosis at their IC_{50} concentrations of 1.62, 1.44 μ M. Treatment of Hela cells with compounds **9** and **13** for 24 h led to 8.47% and 18.99% of apoptotic cells (late apoptosis), respectively, compared to 0.18% of apoptotic cells in the untreated control. Also, there was an increase in the early apoptosis from 0.47% (control) to 2.81% and 5.44% cause by **9** and **13**, respectively with necrosis percent of 1.89 and 2.61% vs. 1.23% produced by DMSO control. It has been noted that the late apoptotic percentages caused by both examined derivatives were higher than that of the early phase which makes it more challenging to recover the apoptotic cells to safe ones. These results revealed that compounds **9** and **13** inhibited cell growth through cell apoptosis induction.

2.7. Molecular docking study

In order to better rationalize how the compounds **2c**, **3f**, **9**, **12** and **13** contributed to the HER2 kinase inhibitory activities, molecular docking simulation studies were carried. The HER2 kinase domain complexed with a ligand was downloaded from the protein databank (PDB ID: 3RCD, <http://www.rcsb.org>). Protein preparation wizard of Schrödinger

Suite (Sastry et al., 2013, Schrödinger, 2018) was used to correct the protein structural file by correcting bond orders, adding any missing hydrogen atoms, and completing unresolved side chains or loops.

The ligands showed good fitting in the active site of HER2 with Glide docking scores in proportion to their biological activities. In general, the docking poses of the ligands demonstrated several good interactions with the DFG region, catalytic loop, activation loop, G-rich loop, phosphate binding loop and α -C helix of HER2 as shown in Table 5. Compound **2c** was docked well in the ligand binding pocket with a Glide docking score of -8.03 kcal/mol. It shows strong hydrogen bonding and cation- π contacts with Lys 753. It has hydrophobic and electrostatic interactions with the surrounding amino acids in the binding site. Compound **3f** showed a docking score of -9.1 kcal/mol (Fig. 8), and a strong hydrogen bonding with Gly 881 in the activation loop. The sulphonyl substituent shifted the structure to some extent inside the binding site. Other hydrophobic and polar contacted are observed with the kinase structural motifs. Compounds **9** (Fig. 9) and **12** (Fig. 10) have docking score of -9.4 and -9.3 kcal/mol, respectively. Both compounds demonstrated strong π - π contacts with Phe 864 in the DFG regions, and multiple polar/



Scheme 3 Synthesis of benzimidazole derivatives conjugated with 2,5-dioxopyrrolidine, 2,5-dioxopyrroline, 1,3-dioxoisindoline, thiazoline and thiazolidine rings (9–13).

nonpolar contacts with the surrounding residues. Compound **13** exhibited strong fitting in the binding site with a Glide score of -9.7 kcal/mol. The compound is strongly interacting with Asn 850 of the catalytic loop, and Asp 863 of the DFG region *via* hydrogen bonding. It shows π - π contacts with Phe 864 of the DFG region (Fig. 11). It could be noted that the most potent HER2 inhibitors **9** and **13** showed the highest negative energy score of -9.4 , -9.7 kcal/mol, respectively, with higher predicted binding affinity than the co-crystallized ligand Erloti-

nib which showed a docking score of -5.8 kcal/mol but lower binding affinity than Lapatinib (docking score = -12 kcal/mol) (Fig. 12).

3. Conclusion

In conclusion, a new series of 6-benzoyl-2-(3,4-dimethoxyphenyl)-1*H*-substituted benzimidazole compounds have been syn-

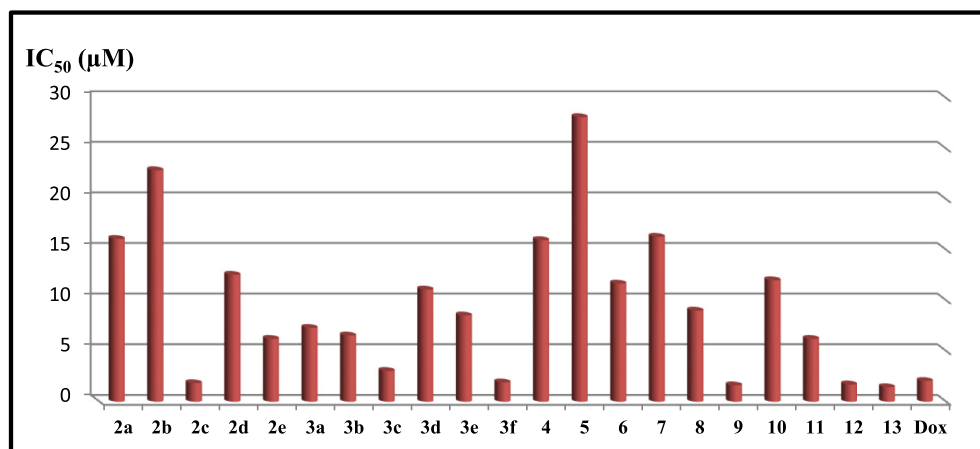


Fig. 3 Anti-cervical cancer evaluation of compounds 2-13 against Hela cell line compared with Doxorubicin.

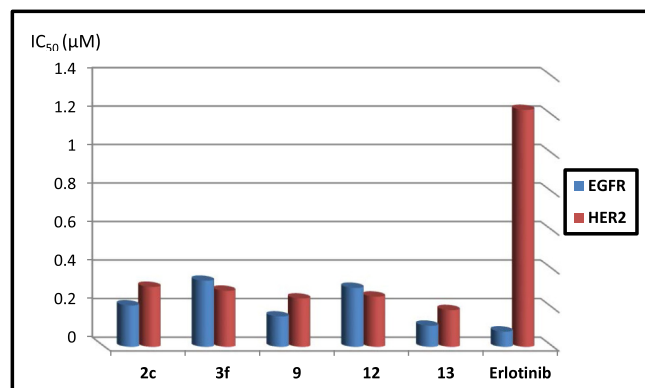
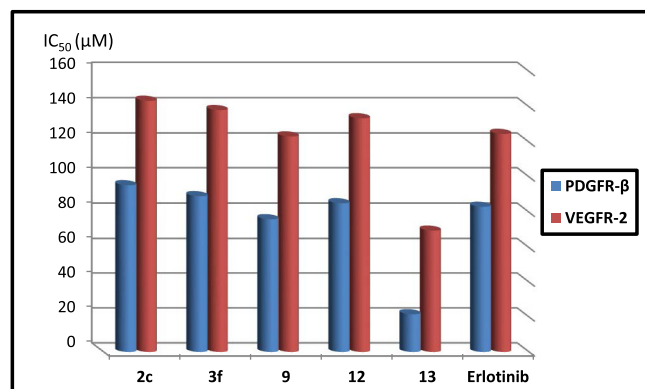
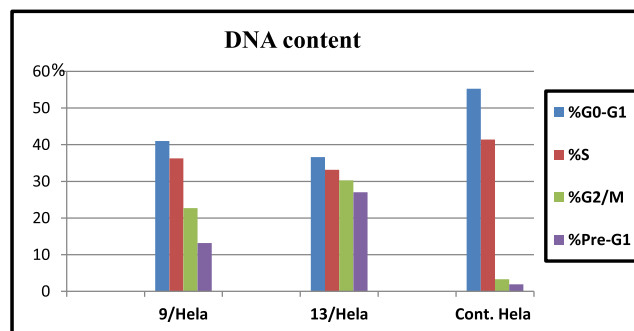
Table 1 Cytotoxic activity of the synthesized benzimidazoles 2-13 on Hela cell line and normal cell line WI-38.

Cpd No.	R/Ar	Hela IC ₅₀ (μM)	WI-38 IC ₅₀ (μM)
2a	H	16.08 ± 0.74	—
2b	3,4-(OCH ₃) ₂	22.87 ± 0.61	—
2c	4-N(CH ₃) ₂	1.84 ± 0.08	12.45 ± 1.41
2d	4-NO ₂	12.53 ± 0.27	—
2e	4-F	6.20 ± 0.18	—
3a	-CO-CH ₃	7.29 ± 0.25	—
3b	-COOC ₂ H ₅	6.53 ± 0.47	—
3c	-NO ₂	3.04 ± 0.07	—
3d	-Br	11.07 ± 0.53	—
3e	-SO ₂ -NH ₂	8.51 ± 0.33	—
3f	-SO ₂ -NH-thiazolyl	1.91 ± 0.13	13.62 ± 1.08
4	-NH ₂	15.96 ± 0.62	—
5	-CO- <i>p</i> -tolyl	28.12 ± 0.11	—
6	-CO-2-furan	11.67 ± 0.46	—
7	-CO-NH ₂	16.29 ± 0.67	—
8	-CS-NH ₂	8.99 ± 0.29	—
9	2,5-dioxypyrrolidine	1.62 ± 0.16	57.38 ± 2.66
10	2,5-dioxypyrroline	6.99 ± 0.42	—
11	1,3-dioxoisindoline	6.23 ± 0.18	—
12	4-methylthiazoline	1.71 ± 0.09	25.11 ± 1.94
13	thiazolidin-4-one	1.44 ± 0.06	77.34 ± 3.61
Doxorubicin		2.05 ± 0.03	79.7 ± 0.07

Table 2 IC₅₀ values of some selected compounds **2c**, **3f**, **9**, **12** and **13** against HER2, EGFR, PDGFR-β and VEGFR-2 kinases.

Cpd No.	EGFR IC ₅₀ (μM)	HER2 IC ₅₀ (μM)	PDGFR-β IC ₅₀ (μM)	VEGFR-2 IC ₅₀ (μM)
2c	0.214 ± 0.008	0.31 ± 0.007	95.31 ± 0.19	143.44 ± 1.1
3f	0.342 ± 0.005	0.29 ± 0.005	89.11 ± 0.17	138.15 ± 2.2
9	0.157 ± 0.007	0.25 ± 0.003	76.09 ± 2.04	123.27 ± 1.7
12	0.305 ± 0.009	0.26 ± 0.006	85.11 ± 0.17	133.54 ± 1.5
13	0.109 ± 0.014	0.19 ± 0.004	21.61 ± 0.47	69.62 ± 1.4
Erlotinib	0.079 ± 0.001	1.23 ± 0.005	83.11 ± 0.17	124.7 ± 1.1
Nazartinib	0.160 ± 0.014	–	–	–

Abbreviations: EGFR, epidermal growth factor receptor; HER, human epidermal growth factor receptor; PDGFR, platelet-derived growth factor receptor; VEGFR, vascular endothelial growth factor receptor.

**Fig. 4** EGFR/HER2 inhibitory effects of compounds **2c**, **3f**, **9**, **12** and **13** compared with Erlotinib.**Fig. 5** PDGFR-β and VEGFR-2 inhibitory effects of compounds **2c**, **3f**, **9**, **12** and **13** compared with Erlotinib.**Fig. 6** Cell Cycle analysis of compounds **9** and **13**.

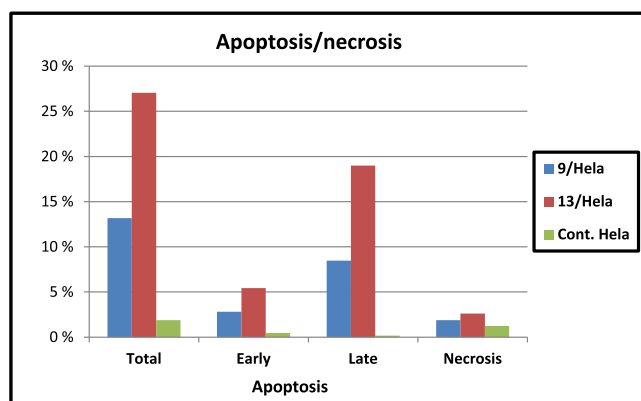
thesized and evaluated as anticancer agents against cervical HeLa cancer cells. The potential inhibitory activity against EGFR/HER2 kinases was evaluated for the most promising cytotoxic derivatives **2c**, **3f**, **9**, **12** and **13**, which exhibited better suppression impact against HER2 than EGFR of IC₅₀ values ranging from 0.19 to 0.31 μM comparing to Erlotinib of IC₅₀; 1.23 μM. The 2,5-dioxopyrrolidine derivative **9** and the thiazolidin-4-one **13** represented promising dual inhibition activity against both EGFR and HER2 kinases. Multi-targeting RTK inhibition was also evaluated against PDGFR-β and VEGFR-2 by compounds **2c**, **3f**, **9**, **12** and **13** as representative examples. Compound **13** demonstrated 3.8 and 1.8 folds more suppression potency than that obtained by Erlotinib as a reference drug. Molecular docking studies exhibited good fitting of compounds **2c**, **3f**, **9**, **12** and **13** in the active site of HER2 with Glide docking scores in proportion to their biological activities. They exhibited strong hydrogen bonding, π-π contacts, hydrophobic and electrostatic interactions with the surrounding amino acids in the binding site of HER2. In addition, cell cycle data exhibited that compounds **9** and **13** caused a pronounced increase in the percentage of HeLa cells at pre-G1 by 13 and 27 folds and at G2/M

Table 3 Results of Cell Cycle analysis of compounds **9** and **13**.

Cpd No.	%G0-G1	%S	%G2/M	%Pre-G1	Comment
9	41.03	36.26	22.71	13.17	PreG1apoptosis&Cell growth arrest@G2/M
13	36.59	33.15	30.26	27.04	PreG1apoptosis&Cell growth arrest@G2/M
Cont. HeLa cells	55.29	41.41	3.3	1.88	

Table 4 Results of Apoptotic activity of compounds **9** and **13**.

Cpd No.	Apoptosis			
	Total	Early	Late	Necrosis
9 /Hela	13.17%	2.81%	8.47%	1.89%
13 /Hela	27.04%	5.44%	18.99%	2.61%
Cont. Hela	1.88%	0.47%	0.18%	1.23%

**Fig. 7** Apoptotic activity of benzimidazole compounds **9** and **13**.

phase by 7 and 10 folds, respectively compared to the untreated Hela cells which confirm a possible role of apoptosis in compounds **9** and **13** induced cancer cell death and cytotoxicity. Compounds **9** and **13** exhibited significant apoptotic activity. Based on the results obtained, it is of interest to continue derivatization and optimization of various benzimidazole series for further kinases inhibition and anticancer studies.

4. Experimental

4.1. Synthesis

The instruments utilized in measuring the melting points, spectral data (IR, Mass, ^1H NMR and ^{13}C NMR) and elemental analysis are cited in details in the [Supplementary material](#).

4.1.1. Synthesis of starting key 1-(6-benzoyl-2-(3,4-dimethoxyphenyl)-1H-benzof[d]imidazol-1-yl)propan-2-one (**1**)

4.1.1.1. Synthesis of (2-(3,4-dimethoxyphenyl)-1H-benzof[d]imidazol-6-yl)(phenyl) methanone (B**).** A stirred mixture of *o*-phenylenediamine **A** (2.12 g, 10 mmol) and 3,4-dimethoxybenzaldehyde (1.67 g, 10 mmol) in dimethylformamide (20 mL) was refluxed for 8 hr. The mixture was then cooled and poured over ice, the precipitated product was collected by filtration, followed by crystallization from methanol to give the pure yellow product **B** (82%); m.p. 116–119 °C. IR (KBr, ν cm^{-1}): 3438 (NH), 3051 (CH-aromatic), 1652 (C = O). ^1H NMR (DMSO d_6 , 400 MHz) δ : 3.91 (s, 3H, OCH₃), 3.93 (s, 3H, OCH₃), 6.68–8.12 (m, 11H, ArH), 9.68 (s, 1H, NH). ^{13}C NMR (DMSO d_6 , 100 MHz) δ : 56.5 (2OCH₃), 111.2, 112.4, 114.9, 119.0, 122.1, 123.3, 128.9, 130.5, 130.7, 131.2, 132.7, 138.4, 145.5, 149.2, 150.9, 152.0, 194.2 (C = O). MS m/z (%): M^+ : 358 (94.5%), ($\text{M} + \text{H}$) $^+$: 359 (1.1%); Anal. Calcd for C₂₂H₁₈N₂O₃ (358.4): C, 73.73; H, 5.06; N, 7.82. Found C, 73.73; H, 5.06; N, 7.82.

4.1.1.2. Synthesis of 1-(6-benzoyl-2-(3,4-dimethoxyphenyl)-1H-benzof[d]imidazol-1-yl)propan-2-one (1**).** A stirred mixture of (2-(3,4-dimethoxyphenyl)-1H-benzof[d]imidazol-6-yl)(phenyl) methanone **B** (3.58 g, 10 mmol) and chloroacetone (0.93 mL, 10 mmol) in dry acetone (30 mL) in the presence of potassium carbonate anhydrous (1.38 g, 10 mmol) was refluxed for 12 hr. The mixture was then cooled and poured over ice, the precipitated product was collected by filtration after neutralization with drops of dilute hydrochloric acid, followed by crystallization from methanol to give the pure yellow product **1** (75%); m.p. 122–125 °C. IR (KBr, ν cm^{-1}): 3051 (CH-aromatic), 1672, 1652 (2C = O). ^1H NMR (DMSO d_6 ,

Table 5 Docking energy scores in kcal/mol for the synthesized compounds **2c**, **3f**, **9**, **12** and **13** in HER2 kinase active site.

Cpd No.	Docking Score (kcal/mol)	Hydrogen-Bond	Aromatic-Bond	pi-pi/cation-pi	Hydrophobic
2c	−8.03	Lys753	Asp863	Lys753	Phe731, Val734, Ala751, Ile752, Leu796, Val797, Leu800, Met801, Phe864, Phe1004
3f	−9.1	Gly881	Asp863, Ser783	–	Ala730, Ala751, Leu800, Met801, Leu852
9	−9.4	–	Ser783, Asp863	Phe864	Phe731, Val734, Ala751, Ile752, Leu796, Leu800, Met801, Phe1004
12	−9.3	Asp863, Lys753	Ser783, Asp863	Phe864	Leu726, Ala730, Phe731, Ala751, Ile752, Met774, Leu785, Leu796, Leu800, Met801, Leu852, Phe1004
13	−9.7	Asn850, Asp863	Asp863, Ser783	Phe864	Ala730, Phe731, Ala751, Ile752, Leu796, Leu800, Met801, Phe1004
Erlotinib	−5.8	Cys805	Asp863	–	Leu726, Val734, Ala751, Ile752, Met774, Phe1004
Lapitanib	−12	Met801, Arg811	Ser783, Gln799, Asp808, Asp863	Phe864	Leu726, Val734, Ala751, Ile752, Met774, Phe1004

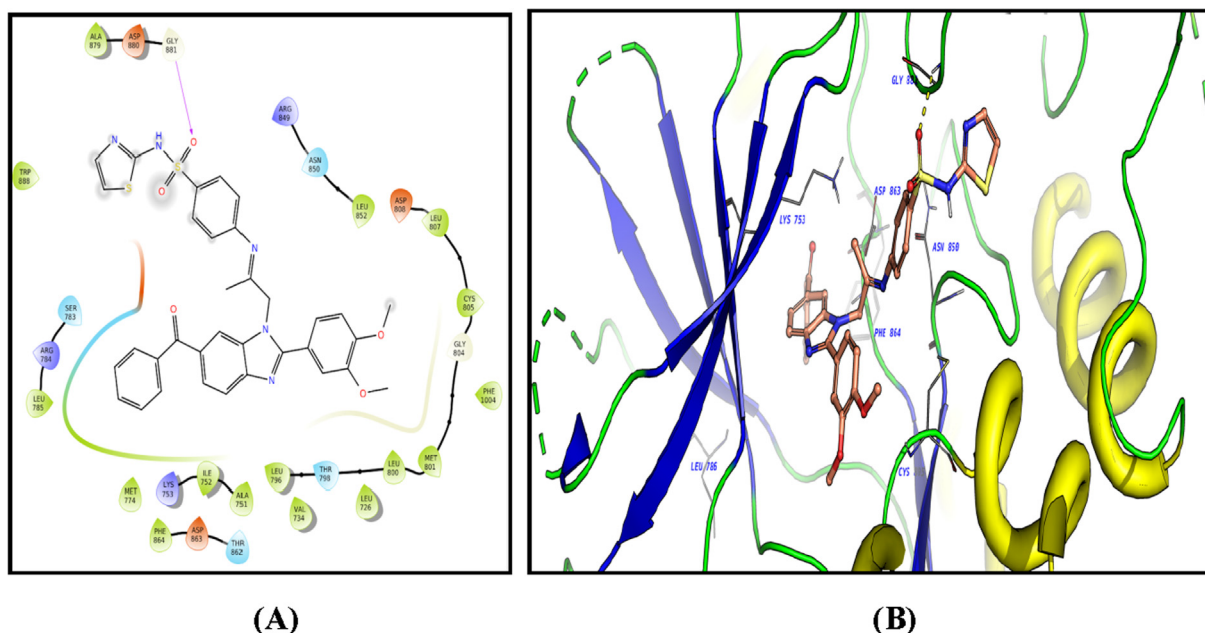


Fig. 8 2D diagram (A) and 3D representation (B) of compound **3f** showing its interaction with the HER2 kinase active site.

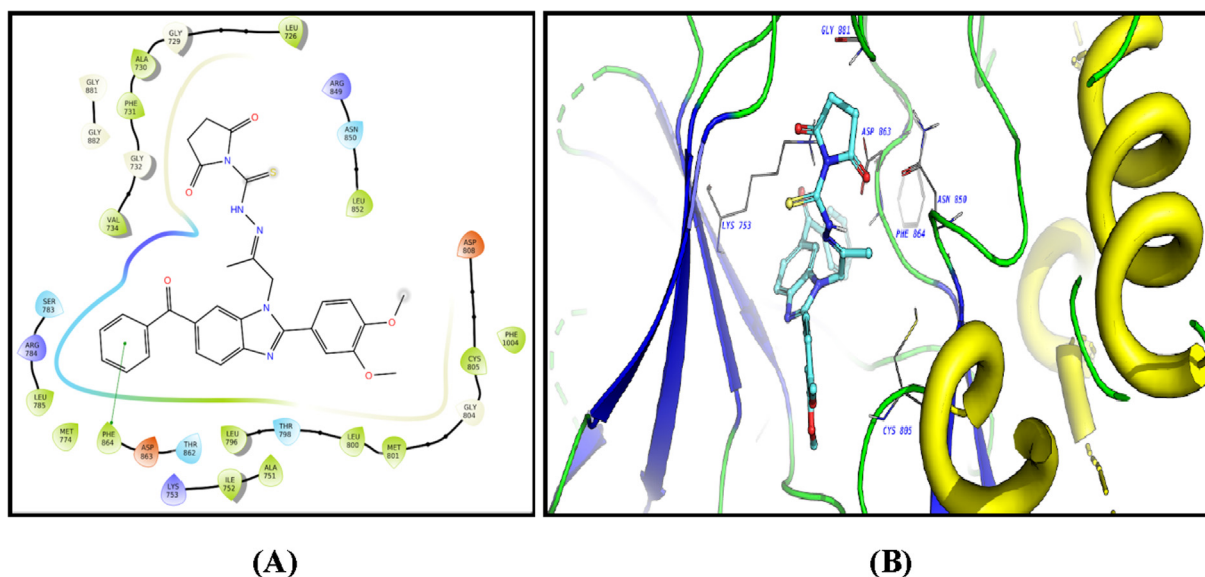


Fig. 9 2D diagram (A) and 3D representation (B) of compound **9** showing its interaction with the HER2 kinase active site.

400 MHz) δ : 2.89 (s, 3H, CH₃), 3.91 (s, 3H, OCH₃), 3.93 (s, 3H, OCH₃), 4.71 (s, 2H, CH₂), 7.1–8.12 (m, 11H, ArH). ¹³C NMR (DMSO *d*₆, 100 MHz) δ : 28.3 (CH₃), 56.5 (2OCH₃), 65.4 (CH₂), 111.2, 112.4, 114.9, 119.0, 122.1, 123.3, 128.9, 130.5, 130.7, 131.2, 132.7, 138.4, 145.5, 149.2, 150.9, 152.0, 194.2 (C = O), 196.2 (C = O). MS *m/z* (%): M⁺: 414 (91.5%), (M + H)⁺: 415 (2.1%); Anal. Calcd for C₂₅H₂₂N₂O₄ (414.4): C, 72.45; H, 5.35; N, 6.76. Found C, 72.45; H, 5.35; N, 6.76.

4.1.2. General method for the synthesis of (*E*)-1-(6-benzoyl-2-(3,4-dimethoxyphenyl)-1*H*-benzo[*d*]imidazol-1-yl)-4-(substituted)phenylbut-3-en-2-one compounds (**2a-2e**)

A mixture of compound **1** (4 g, 10 mmol) and the appropriate aromatic aldehydes, namely; benzaldehyde, 3,4-dimethoxybenzaldehyde, 4-*N*-dimethylbenzaldehyde, 4-nitrobenzaldehyde and 4-fluorobenzaldehyde, (10 mmol) in absolute ethanol (30 mL) containing few drops of piperidine was refluxed for 2–4 h. After completion of the reaction, the solu-

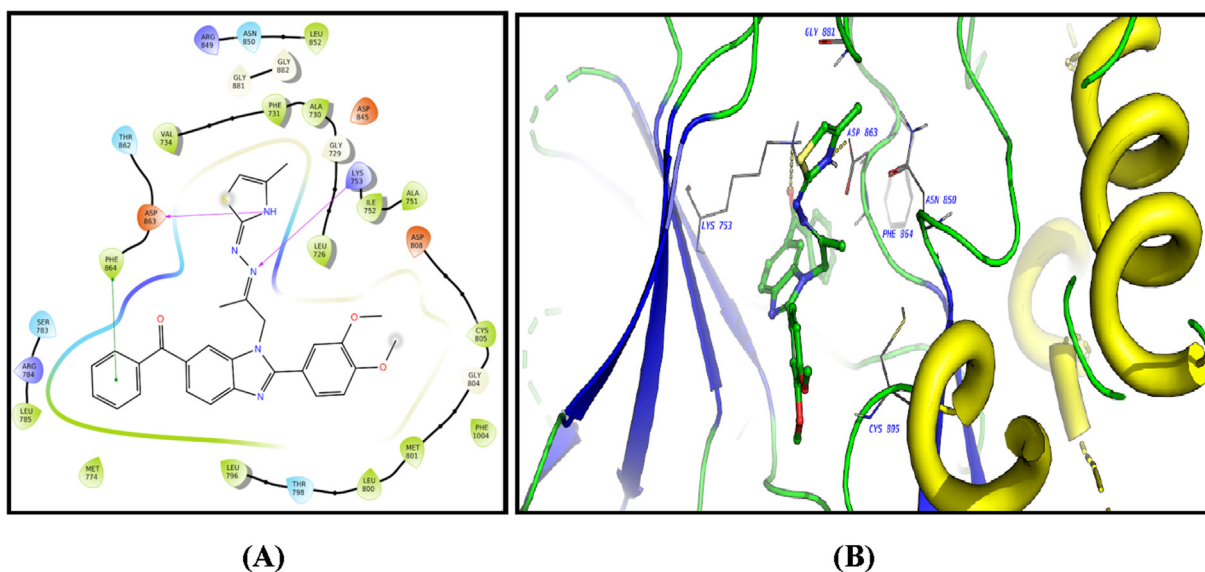


Fig. 10 2D diagram (A) and 3D representation (B) of compound 12 showing its interaction with the HER2 kinase active site.

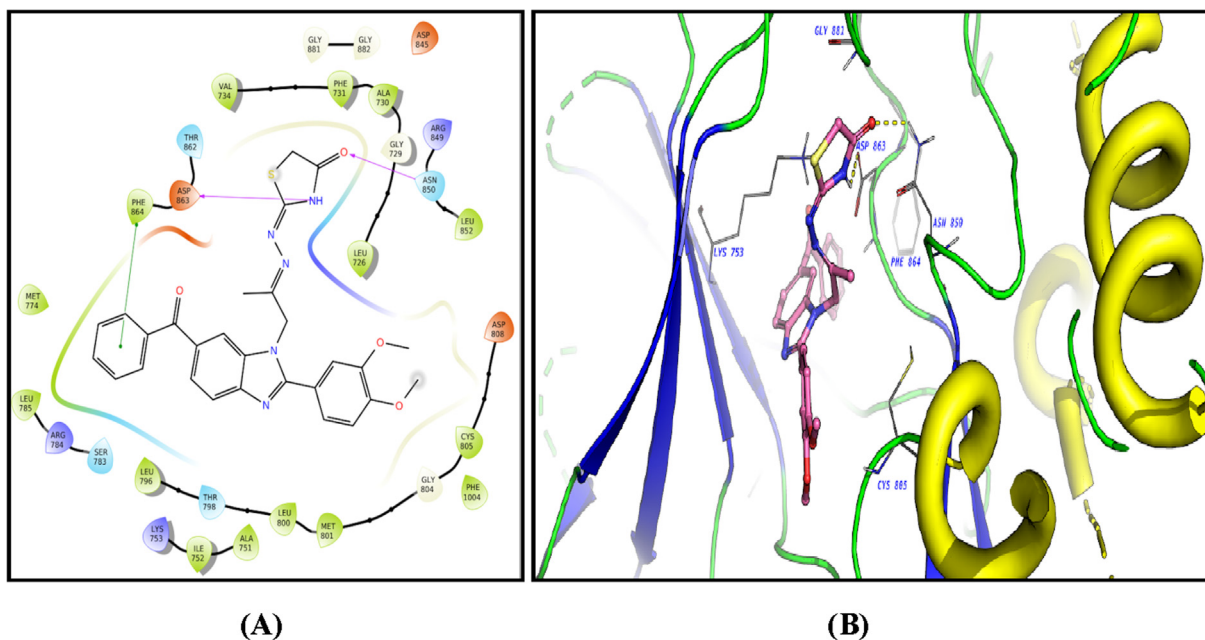


Fig. 11 2D diagram (A) and 3D representation (B) of compound 13 showing its interaction with the HER2 kinase active site.

tion mixture was cooled and triturated with ethanol, then filtered, and crystallized from methanol to give the corresponding chalcones **2a-2e**.

4.1.2.1. (*E*)-1-(6-benzoyl-2-(3,4-dimethoxyphenyl)-1H-benzimidazol-1-yl)-4-phenylbut-3-en-2-one (**2a**). Yellowish white solid, yield: 65%, m.p. 212–215 °C. IR (KBr, ν cm^{-1}): 3051 (CH-aromatic), 1670, 1652 (2C = O). ^1H NMR (DMSO d_6 , 400 MHz) δ : 3.93, 3.95 (2 s, 6H, 2OCH₃), 5.18 (s, 2H, N-CH₂), 6.92 (d, 1H, =CH *a*, J = 9.6 Hz), 7.56–7.77 (m, 17H, =CH β & ArH). ^{13}C NMR (DMSO d_6 , 100 MHz) δ : 56.5 (2OCH₃), 64.1 (CH₂), 111.2, 112.4, 112.5, 113.1, 113.5, 117.9, 122.0, 122.3, 122.6, 124.9, 126.2, 128.9,

129.5, 130.5, 131.0, 133.7, 136.7, 138.4, 146.5, 149.2, 150.9, 155.0, 156.0 (Ar-C), 196.2 (C = O). MS m/z (%): M^+ : 502 (84.5%), ($\text{M} + \text{H}$) $^+$: 503 (1.1%); Anal. Calcd for C₃₂H₂₆N₂O₄ (502.57): C, 76.48; H, 5.21; N, 5.57. Found C, 76.48; H, 5.20; N, 5.57.

4.1.2.2. (*E*)-1-(6-benzoyl-2-(3,4-dimethoxyphenyl)-1H-benzimidazol-1-yl)-4-(3,4-dimethoxyphenyl)but-3-en-2-one (**2b**). Yellowish white solid, yield: 65%, m.p. 140–142 °C. IR (KBr, ν cm^{-1}): 3049 (CH-aromatic), 1672, 1640 (2C = O). ^1H NMR (DMSO d_6 , 400 MHz): δ 3.81, 3.93, 3.95 (3 s, 12H, 4OCH₃), 5.28 (s, 2H, N-CH₂), 7.00 (d, 1H, =CH *a*, J = 9.6 Hz), 7.22–8.21 (m, 15H, =CH β & ArH). ^{13}C

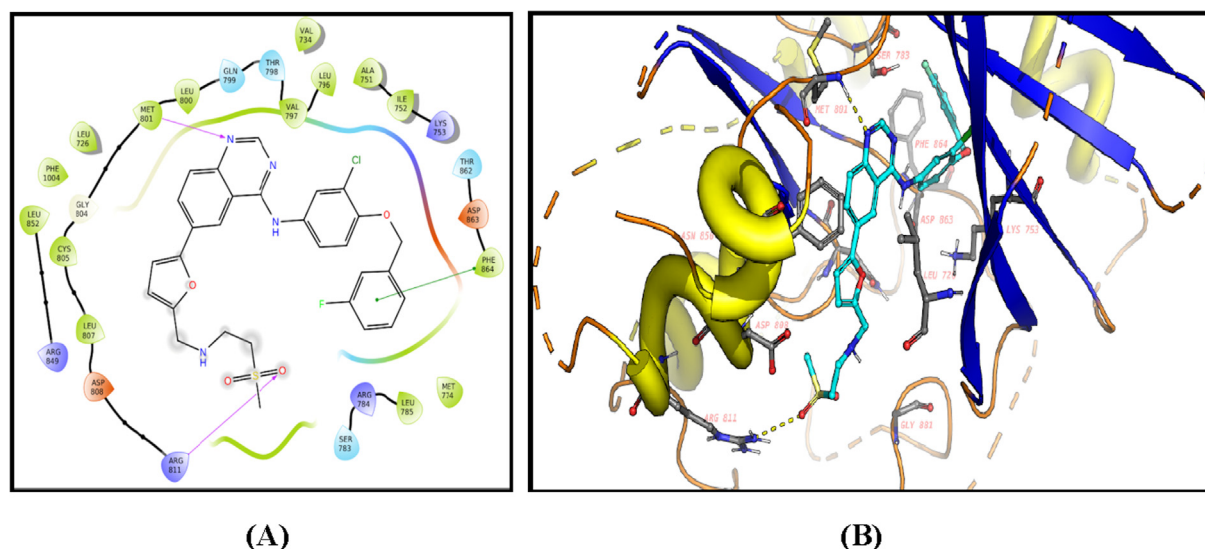


Fig. 12 2D diagram (A) and 3D representation (B) of Lapatinib showing its interaction with the HER2 kinase active site.

NMR (DMSO d_6 , 100 MHz) δ : 56.1 (4OCH₃), 64.1 (CH₂), 111.2, 112.4, 112.5, 113.1, 113.5, 117.9, 122.0, 122.3, 122.6, 124.9, 126.2, 128.9, 129.5, 130.5, 131.0, 133.7, 136.7, 138.4, 146.5, 149.2, 150.9, 155.0, 156.0 (Ar-C), 196.2 (C = O). MS m/z (%): M^+ : 562 (64.5%), ($M + H$)⁺: 563 (1.1%); Anal. Calcd for C₃₄H₃₀N₂O₆ (562.62): C, 72.58; H, 5.37; N, 4.98. Found C, 72.58; H, 5.37; N, 4.98.

4.1.2.3. (*E*)-1-(6-benzoyl-2-(3,4-dimethoxyphenyl)-1H-benzo[d]imidazol-1-yl)-4-(4-(dimethylamino)phenyl)but-3-en-2-one (2c). Brownish white solid, yield: 65%, m.p. 197–199 °C. IR (KBr, ν cm⁻¹): 3050 (CH-aromatic), 1670, 1650 (2C = O). ¹H NMR (DMSO d_6 , 400 MHz): δ 2.41 (s, 6H, -N(CH₃)₂), 3.93, 3.95 (2 s, 6H, 2OCH₃), 5.18 (s, 2H, N-CH₂), 6.92 (d, 1H, =CH- α , J = 7.6 Hz), 7.22–8.59 (m, 16H, =CH- β & ArH). ¹³C NMR (DMSO d_6 , 100 MHz) δ 45.1 (N-CH₃)₂, 56.1 (2OCH₃), 64.1 (CH₂), 111.2, 112.2, 112.5, 113.0, 113.4, 118.9, 122.0, 122.1, 122.2, 124.9, 126.2, 128.9, 129.9, 130.5, 131.7, 133.7, 136.7, 138.4, 146.1, 149.2, 150.9, 154.0, 156.0 (Ar-C), 196.2 (C = O). MS m/z (%): M^+ : 545 (44.5%); Anal. Calcd for C₃₄H₃₁N₃O₄ (545.64): C, 74.84; H, 5.73; N, 7.70. Found C, 74.84; H, 5.73; N, 7.70.

4.1.2.4. (*E*)-1-(6-benzoyl-2-(3,4-dimethoxyphenyl)-1H-benzo[d]imidazol-1-yl)-4-(4-nitrophenyl) but-3-en-2-one (2d). Yellow solid, yield: 63%, m.p. 195–197 °C. IR (KBr, ν cm⁻¹): 3049 (CH-aromatic), 1665, 1643 (2C = O), 1553, 1320 (NO₂). ¹H NMR (DMSO d_6 , 400 MHz): δ 3.92, 3.95 (2 s, 6H, 2OCH₃), 5.12 (s, 2H, N-CH₂), 7.23 (d, 1H, =CH α , J = 7.6 Hz), 7.62–8.45 (m, 16H, =CH β & ArH). ¹³C NMR (DMSO d_6 , 100 MHz) δ 56.1 (2OCH₃), 64.1 (CH₂), 111.2, 112.2, 112.5, 113.0, 113.4, 118.9, 122.0, 122.1, 122.2, 124.9, 126.2, 128.9, 129.9, 130.5, 131.7, 133.7, 136.7, 138.4, 146.1, 149.2, 150.9, 154.0, 156.0 (Ar-C), 196.2 (C = O). MS m/z (%): M^+ : 547 (44.5%); Anal. Calcd for C₃₂H₂₅N₃O₆ (547.57): C, 70.19; H, 4.60; N, 7.67. Found C, 70.19; H, 4.60; N, 7.67.

4.1.2.5. (*E*)-1-(6-benzoyl-2-(3,4-dimethoxyphenyl)-1H-benzo[d]imidazol-1-yl)-4-(4-fluorophenyl)but-3-en-2-one (2e). Gray white solid, yield: 65%, m.p. 132–134 °C. IR (KBr, ν cm⁻¹): 3052 (CH-aromatic), 1670, 1645 (2C = O). ¹H NMR (DMSO d_6 , 400 MHz): δ 3.75, 3.87 (2 s, 6H, 2OCH₃), 5.17 (s, 2H, N-CH₂), 7.20 (d, 1H, =CH α , J = 7.6 Hz), 7.41–7.90 (m, 16H, =CH β & ArH). ¹³C NMR (DMSO d_6 , 100 MHz) δ 56.1 (2OCH₃), 64.1 (CH₂), 111.2, 112.2, 112.5, 113.0, 113.4, 118.9, 122.0, 122.1, 122.2, 124.9, 126.2, 128.9, 129.9, 130.5, 131.7, 133.7, 136.7, 138.4, 146.1, 149.2, 150.9, 154.0, 156.0 (Ar-C), 196.2 (C = O). MS m/z (%): M^+ : 520 (73.5%); Anal. Calcd for C₃₂H₂₅FN₂O₄ (520.56): C, 73.83; H, 4.84; N, 5.38. Found C, 73.83; H, 4.84; N, 5.38.

4.1.3. General method for the synthesis of Schiff bases (3a–3f)

A mixture of compound **1** (4 g, 10 mmol) and various aromatic amines such as 4-aminoacetophenone, ethyl 4-aminobenzoate, 4-nitroaniline, 4-bromoaniline, 4-aminobenzenesulfonamide and sulfathiazole (10 mmol) in ethanol (30 mL) containing few drops of glacial acetic acid was heated at refluxing temperature for 12 h. The mixture solution was left to cool and the precipitated solid was filtered and crystallized from DMF/EtOH to give the corresponding Schiff compounds **3a–3f**.

4.1.3.1. (*E*)-1-(4-((1-(6-benzoyl-2-(3,4-dimethoxyphenyl)-1H-benzo[d]imidazol-1-yl) propan-2-ylidene)amino)phenyl)ethanol-1-one (3a). Brownish white solid, yield: 70%, m.p. 125–127 °C. IR (KBr, ν cm⁻¹): 3050 (CH-aromatic), 1704, 1665 (2C = O). ¹H NMR (DMSO d_6 , 400 MHz): δ 2.25 (s, 3H, CH₃), 2.41 (s, 3H, -COCH₃), 3.92, 3.95 (2 s, 6H, 2OCH₃), 5.18 (s, 2H, N-CH₂), 6.92–8.59 (m, 15H, ArH). ¹³C NMR (DMSO d_6 , 100 MHz) δ 14.1 (CH₃), 27.2 (CO-CH₃), 56.0 (2OCH₃), 57.6 (CH₂), 112.2, 112.6, 112.9, 113.4, 118.9, 122.0, 122.1, 122.2, 124.9, 128.9, 129.9, 130.1, 131.7, 132.7, 136.7, 138.4, 146.1, 149.2, 150.9, 154.0 (Ar-C), 156.0 (C = N), 196.1, 203.1 (2C = O). MS m/z (%): M^+ : 531 (44.5%); Anal.

Calcd for C₃₃H₂₉N₃O₄ (531.61): C, 74.56; H, 5.50; N, 7.90. Found C, 74.56; H, 5.50; N, 7.90.

4.1.3.2. Ethyl (*E*)-4-((1-(6-benzoyl-2-(3,4-dimethoxyphenyl)-1*H*-benzo[d]imidazol-1-yl)propan-2-ylidene)amino)benzoate (**3b**). Gray white solid, yield: 65%, m.p. 143–145 °C. IR (KBr, ν cm⁻¹): 3072 (CH-aromatic), 1680, 1665 (2C = O). ¹H NMR (DMSO *d*₆, 400 MHz): δ 1.52 (t, 3H, -CH₂CH₃, *J* = 7.6 Hz), 2.04 (s, 3H, CH₃), 3.92, 3.95 (2 s, 6H, 2OCH₃), 4.25 (q, 4H, -CH₂CH₃, *J* = 7.6 Hz, N-CH₂), 5.18 (s, 2H, N-CH₂), 6.92–8.59 (m, 15H, ArH). ¹³C NMR (DMSO *d*₆, 100 MHz) δ 14.1 (CH₃), 27.2 (CH₂-CH₃), 56.0 (2OCH₃), 57.6 (CH₂), 60.9 (CH₂), 112.2, 112.6, 112.9, 113.4, 118.9, 122.0, 122.1, 122.2, 124.9, 128.9, 129.9, 130.1, 131.7, 132.7, 136.7, 138.4, 146.1, 149.2, 150.9, 154.0 (Ar-C), 156.0 (C = N), 196.1, 203.1 (2C = O). MS *m/z* (%): M⁺: 561 (66.5%); Anal. Calcd for C₃₄H₃₁N₃O₅ (561.64): C, 72.71; H, 5.56; N, 7.48. Found C, 72.71; H, 5.56; N, 7.48.

4.1.3.3. (*E*)-2-(3,4-dimethoxyphenyl)-1-(2-((4-nitrophenyl)imino)propyl)-1*H*-benzo[d]imidazol-6-yl(phenyl)methanone (**3c**). Yellow solid, yield: 65%, m.p. 117–119 °C. IR (KBr, ν cm⁻¹): 3055 (CH-aromatic), 1669 (C = O), 1550, 1325 (NO₂). ¹H NMR (DMSO *d*₆, 400 MHz): δ 2.01 (s, 3H, CH₃), 3.92, 3.95 (2 s, 6H, 2OCH₃), 5.18 (s, 2H, N-CH₂), 6.92–8.59 (m, 15H, ArH). ¹³C NMR (DMSO *d*₆, 100 MHz) δ 26.0 (CH₃), 56.3 (2OCH₃), 57.5 (CH₂), 112.2, 112.2, 113.0, 113.4, 119.9, 122.0, 122.3, 123.2, 124.9, 128.8, 129.9, 130.2, 131.7, 132.7, 136.7, 139.4, 145.1, 149.3, 152.9, 154.0, 156.0 (Ar-C), 196.1 (C = O). MS *m/z* (%): M⁺: 534 (44.5%); Anal. Calcd for C₃₁H₂₆N₄O₅ (534.57): C, 69.65; H, 4.90; N, 10.48. Found C, 69.65; H, 4.90; N, 10.48.

4.1.3.4. (*E*)-1-(2-((4-bromophenyl)imino)propyl)-2-(3,4-dimethoxyphenyl)-1*H*-benzo[d]imidazol-6-yl(phenyl)methanone (**3d**). Orange solid, yield: 65%, m.p. 162–164 °C. IR (KBr, ν cm⁻¹): 3155 (CH-aromatic), 1665 (C = O). ¹H NMR (DMSO *d*₆, 400 MHz): δ 2.01 (s, 3H, CH₃), 3.92, 3.95 (2 s, 6H, 2OCH₃), 5.15 (s, 2H, N-CH₂), 6.92–8.59 (m, 15H, ArH). ¹³C NMR (DMSO *d*₆, 100 MHz) δ 26.0 (CH₃), 56.3 (2OCH₃), 57.5 (CH₂), 112.2, 112.2, 113.0, 113.4, 119.9, 122.0, 122.3, 123.2, 124.9, 128.8, 129.9, 130.2, 131.7, 132.7, 136.7, 139.4, 145.1, 149.3, 152.9, 154.0, 156.0 (Ar-C), 196.1 (C = O). MS *m/z* (%): M⁺: 568 (50%), (M + 2)⁺: 370 (49%); Anal. Calcd for C₃₁H₂₆BrN₃O₃ (568.47): C, 65.50; H, 4.61; N, 7.39. Found C, 65.50; H, 4.61; N, 7.39.

4.1.3.5. (*E*)-4-((1-(6-benzoyl-2-(3,4-dimethoxyphenyl)-1*H*-benzo[d]imidazol-1-yl)propan-2-ylidene)amino)benzenesulfonamide (**3e**). Gray white solid, yield: 66%, m.p. 103–105 °C. IR (KBr, ν cm⁻¹): 3051 (CH-aromatic), 1663 (C = O), 1357, 1134 (SO₂). ¹H NMR (DMSO *d*₆, 400 MHz): δ 2.04 (s, 3H, CH₃), 3.92, 3.95 (2 s, 6H, 2OCH₃), 5.15 (s, 2H, N-CH₂), 6.92–8.59 (m, 15H, ArH), 9.25 (s, 2H, NH₂, D₂O exchangeable). ¹³C NMR (DMSO *d*₆, 100 MHz) δ 26.0 (CH₃), 56.3 (2OCH₃), 57.5 (CH₂), 112.2, 112.2, 113.0, 113.4, 119.9, 122.0, 122.3, 123.2, 124.9, 128.8, 129.9, 130.2, 131.7, 132.7, 136.7, 139.4, 145.1, 149.3, 152.9, 154.0, 156.0 (Ar-C), 196.1 (C = O). MS *m/z* (%): M⁺: 568 (94%); Anal. Calcd for C₃₁H₂₈N₄O₅S (568.65): C, 65.48; H, 4.96; N, 9.85. Found C, 65.48; H, 4.96; N, 9.85.

4.1.3.6. (*E*)-2-(3,4-dimethoxyphenyl)-1-(2-((4-(thiazol-2-ylsulfonyl)phenyl)imino)propyl)-1*H*-benzo[d]imidazol-6-yl(phenyl)methanone (**3f**). White solid, yield: 62%, m.p. 113–115 °C. IR (KBr, ν cm⁻¹): 3435 (NH), 3065 (CH-aromatic), 1663 (C = O), 1355, 1130 (SO₂). ¹H NMR (DMSO *d*₆, 400 MHz): δ 1.94 (s, 3H, CH₃), 3.91, 3.95 (2 s, 6H, 2OCH₃), 5.16 (s, 2H, N-CH₂), 6.92–8.63 (m, 17H, ArH), 11.31 (s, 1H, NH, D₂O exchangeable). MS *m/z* (%): M⁺: 651 (34%); Anal. Calcd for C₃₄H₂₉N₅O₅S₂ (651.74): C, 62.66; H, 4.49; N, 10.75. Found C, 62.66; H, 4.49; N, 10.75.

4.1.4. General method for synthesis of the hydrazone derivatives (**4–6**)

A mixture of compound **1** (4 g, 10 mmol) and nucleophilic compounds such as hydrazine hydrate (98%), *p*-toluic hydrazide and 2-furoic acid hydrazide (10 mmol) in ethanol (30 mL) was heated at refluxing temperature for 12 h. The reaction mixture was left to cool. The obtained solid was filtered and crystallized from methanol to give the corresponding compounds **4–6**, respectively.

4.1.4.1. (*E*)-2-(3,4-dimethoxyphenyl)-1-(2-hydrazineylidene)propyl)-1*H*-benzo[d]imidazol-6-yl(phenyl)methanone (**4**). White solid, yield: 67%, m.p. 103–105 °C. IR (KBr, ν cm⁻¹): 3423, 3252 (NH₂), 3037 (CH-aromatic), 1650 (C = O). ¹H NMR (DMSO *d*₆, 400 MHz): δ 1.91 (s, 3H, CH₃), 3.94, 3.85 (2 s, 6H, 2OCH₃), 5.28 (s, 2H, N-CH₂), 4.78 (s, 2H, NH₂, D₂O exchangeable), 7.03–8.31 (m, 11H, ArH). ¹³C NMR (DMSO *d*₆, 100 MHz) δ : 18.3 (CH₃), 56.5 (2OCH₃), 65.4 (CH₂), 111.2, 112.4, 114.9, 119.0, 122.1, 123.3, 128.9, 130.5, 130.7, 131.2, 132.7, 138.4, 146.5, 149.2, 152.9, 155.0, 194.2 (C = O). MS *m/z* (%): M⁺: 428 (29.5%); Anal. Calcd for C₂₅H₂₄N₄O₃ (428.495): C, 70.08; H, 5.65; N, 13.08. Found C, 70.08; H, 5.65; N, 13.07.

4.1.4.2. (*E*)-*N'*-(1-(6-benzoyl-2-(3,4-dimethoxyphenyl)-1*H*-benzo[d]imidazol-1-yl)propan-2-ylidene)-4-methylbenzohydrazide (**5**). Gray white solid, yield: 65%, m.p. 195–197 °C. IR (KBr, ν cm⁻¹): 3423 (NH), 3037 (CH-aromatic), 1650, 1643 (2C = O). ¹H NMR (DMSO *d*₆, 400 MHz): δ 2.25 (s, 3H, CH₃), 2.41 (s, 3H, CH₃), 3.93, 3.95 (2 s, 6H, 2OCH₃), 5.18 (s, 2H, N-CH₂), 6.92–8.59 (m, 15H, ArH), 11.50 (s, 1H, NH, D₂O exchangeable). ¹³C NMR (DMSO *d*₆, 100 MHz) δ 21.4, 29.9 (2CH₃), 56.0 (2OCH₃), 58.9 (CH₂), 85.8, 111.9, 112.1, 112.2, 112.8, 122.2, 122.2, 122.3, 128.1, 128.9, 129.2, 129.4, 130.9, 131.3, 142.2, 149.0, 150.7 (Ar-C), 178.3, 198.5 (2C = O). MS *m/z* (%): M⁺: 546 (44.5%); Anal. Calcd for C₃₃H₃₀N₄O₄ (546.63): C, 72.51; H, 5.53; N, 10.25. Found: C, 72.51; H, 5.53; N, 10.25.

4.1.4.3. (*E*)-*N'*-(1-(6-benzoyl-2-(3,4-dimethoxyphenyl)-1*H*-benzo[d]imidazol-1-yl)propan-2-ylidene) furan-2-carbohydrazide (**6**). Gray white solid, yield: 60%, m.p. 235–237 °C. IR (KBr, ν cm⁻¹): 3440 (NH), 3050 (CH-aromatic), 1655, 1645 (2C = O). ¹H NMR (DMSO *d*₆, 400 MHz): δ 2.41 (s, 3H, CH₃), 3.93, 3.95 (2 s, 6H, 2OCH₃), 5.18 (s, 2H, N-CH₂), 7.21–7.95 (m, 14H, ArH), 10.42 (s, 1H, NH, D₂O exchangeable). MS *m/z* (%): M⁺: 522 (49%); Anal. Calcd for C₃₀H₂₆N₄O₅ (522.56): C, 68.95; H, 5.02; N, 10.72. Found: C, 68.95; H, 5.02; N, 10.73.

4.1.5. (*E*)-2-(1-(6-benzoyl-2-(3,4-dimethoxyphenyl))-1*H*-benzo[d]imidazol-1-yl)propan-2-ylidene)hydrazine-1-carboxamide (**7**)

A mixture of compound **1** (4.10 g, 10 mmol), semicarbazide hydrochloride (1.11 g, 10 mmol) and sodium acetate (1.64 g, 20 mmol) in ethanol (20 mL) was stirred for 1 h at room temperature, then refluxed for 3 h. The formed precipitate was filtered, washed several times with water, dried, and recrystallized from ethanol to give the compound **7** as white solid.

Yield: 70%, m.p. 282–284 °C. IR (KBr, ν cm⁻¹): 3440, 3350, 3235 (NH₂), 3050 (CH-aromatic), 1650, 1645 (2C = O). ¹H NMR (DMSO *d*₆, 400 MHz): δ 1.91 (s, 3H, CH₃), 3.73, 3.84 (2 s, 6H, 2OCH₃), 5.45 (s, 2H, NH₂, D₂O exchangeable), 5.65 (s, 2H, N-CH₂), 7.11–7.85 (m, 11H, ArH), 9.52 (s, 1H, NH, D₂O exchangeable). MS *m/z* (%): M⁺: 471 (60%); Anal. Calcd for C₂₆H₂₅N₅O₄ (471.52): C, 66.23; H, 5.34; N, 14.85. Found: C, 66.24; H, 5.34; N, 14.85.

4.1.6. (*E*)-2-(1-(6-benzoyl-2-(3,4-dimethoxyphenyl))-1*H*-benzo[d]imidazol-1-yl)propan-2-ylidene) hydrazine-1-carbothioamide (**8**)

A mixture of **1** (4.10 g, 10 mmol), thiosemicarbazide (1 g, 10 mmol) in absolute ethanol (15 mL) containing a few drops of concentrated hydrochloric acid was refluxed for 3 h. The formed precipitate was filtered, dried, and crystallized from ethanol to give the compound **8** as yellowish white solid.

Yield: 73%, m.p. 233–235 °C. IR (KBr, ν cm⁻¹): 3440, 3360, 3240 (NH₂, NH), 3050 (CH-aromatic), 1665 (C = O), 1110 (C = S). ¹H NMR (DMSO *d*₆, 400 MHz): δ 1.91 (s, 3H, CH₃), 3.91, 3.94 (2 s, 6H, 2OCH₃), 5.45 (s, 2H, N-CH₂), 5.75 (s, 2H, NH₂, D₂O exchangeable), 7.01–7.95 (m, 11H, ArH), 10.42 (s, 1H, NH, D₂O exchangeable). ¹³C NMR (DMSO *d*₆, 100 MHz) δ 22.1 (CH₃), 56.0 (2OCH₃), 57.6 (CH₂), 112.1, 112.6, 128.7, 128.8, 128.9, 129.0, 130.1, 130.3, 137.7, 143.1, 143.9, 149.2, 149.5, 150.9, 154.0, 156.0 (Ar-C), 185.1 (C = O), 187.2 (C = S). MS *m/z* (%): M⁺: 487 (90%); Anal. Calcd for C₂₆H₂₅N₅O₃S (487.58): C, 64.05; H, 5.17; N, 14.36. Found: 64.05; H, 5.18; N, 14.36.

4.1.7. General method for synthesis of 2,5-dioxopyrrolidine, 2,5-dioxopyrroline and 1,3-dioxoisindoline derivatives (**9–11**)

To a solution of compound **8** (4.8 g, 10 mmol) in glacial acetic acid, succinic anhydride, maleic anhydride or phthalic anhydride (10 mmol) was added. The mixture was refluxed for 8 h, then poured onto ice/H₂O. The formed precipitate was filtered, washed with water and recrystallized from dioxane to give the corresponding derivatives **9–11**.

4.1.7.1. (*E*)-*N'*-(1-(6-benzoyl-2-(3,4-dimethoxyphenyl))-1*H*-benzo[d]imidazol-1-yl) propan-2-ylidene)-2,5-dioxopyrrolidine-1-carbothiohydrazide (**9**). White solid, yield: 73%, m.p. 113–115 °C. IR (KBr, ν cm⁻¹): 3335 (NH), 3150 (CH-aromatic), 1688, 1655 (3C = O), 1125 (C = S). ¹H NMR (DMSO *d*₆, 400 MHz): δ 1.92 (s, 3H, CH₃), 2.75 (t, 4H, pyrrolidine-(CH₂)₂), 3.85, 3.90 (2 s, 6H, 2OCH₃), 5.45 (s, 2H, N-CH₂), 7.11–7.75 (m, 11H, ArH), 12.12 (s, 1H, NH, D₂O exchangeable). ¹³C NMR (DMSO *d*₆, 100 MHz) δ 26.7 (CH₃), 29.7 (pyrrolidine-(CH₂)₂), 56.3 (2OCH₃), 57.6 (CH₂), 112.0, 112.5, 112.9, 117.9, 120.5, 122.1, 127.8, 128.7, 129.9, 130.1, 131.9, 132.7, 146.3, 149.2, 153.9, 156.0, 159.0 (Ar-C),

186.1 (C = S), 196.5, 203.3 (2C = O). MS *m/z* (%): M⁺: 569 (40%); Anal. Calcd for: C₃₀H₂₇N₅O₅S (569.64): C, 63.26; H, 4.78; N, 12.29. Found: C, 63.25; H, 4.78; N, 12.29.

4.1.7.2. (*E*)-*N'*-(1-(6-benzoyl-2-(3,4-dimethoxyphenyl))-1*H*-benzo[d]imidazol-1-yl) propan-2-ylidene)-2,5-dioxo-2,5-dihydro-1*H*-pyrrole-1-carbothiohydrazide (**10**). White solid, yield: 73%, m.p. 190–192 °C. IR (KBr, ν cm⁻¹): 3440 (NH), 3150 (CH-aromatic), 1670, 1655 (3C = O), 1123 (C = S). ¹H NMR (DMSO *d*₆, 400 MHz): δ 1.81 (s, 3H, CH₃), 3.92, 3.95 (2 s, 6H, 2OCH₃), 5.41 (s, 2H, N-CH₂), 7.01–7.70 (m, 13H, ArH), 12.21 (s, 1H, NH, D₂O exchangeable). MS *m/z* (%): M⁺: 567 (30%); Anal. Calcd for: C₃₀H₂₅N₅O₅S (567.62): C, 63.48; H, 4.44; N, 12.34. Found: C, 63.48; H, 4.45; N, 12.34.

4.1.7.3. (*E*)-*N'*-(1-(6-benzoyl-2-(3,4-dimethoxyphenyl))-1*H*-benzo[d]imidazol-1-yl) propan-2-ylidene)-1,3-dioxoisindoline-2-carbothiohydrazide (**11**). White solid, yield: 71%, m.p. 190–192 °C. IR (KBr, ν cm⁻¹): 3440 (NH), 3155 (CH-aromatic), 1672, 1650 (3C = O), 1125 (C = S). ¹H NMR (DMSO *d*₆, 400 MHz): δ 1.91 (s, 3H, CH₃), 3.80, 3.92 (2 s, 6H, 2OCH₃), 5.65 (s, 2H, N-CH₂), 7.01–7.70 (m, 15H, ArH), 12.21 (s, 1H, NH, D₂O exchangeable). MS *m/z* (%): M⁺: 617 (40%); Anal. Calcd for: C₃₄H₂₇N₅O₅S (617.68): C, 66.11; H, 4.41; N, 11.34. Found: C, 66.11; H, 4.41; N, 11.35.

4.1.8. General procedure for synthesis of 4-methylthiazoline and thiazolidin-4-one compounds (**12, 13**)

A mixture of compound **8** (4.8 g, 10 mmol) and chloroacetone or ethyl bromoacetate (10 mmol) in absolute ethanol (20 mL) containing sodium acetate anhydrous (1.64 g, 20 mmol) was heated at the refluxing temperature for 10 h. The formed precipitate was filtered, washed with water, dried, and recrystallized from the proper solvent to accomplish the target derivatives **12, 13**, respectively.

4.1.8.1. (2-(3,4-Dimethoxyphenyl)-1-((*E*)-2-((*E*)-4-methylthiazol-2(3*H*)-ylidene) hydrazineylidene)propyl)-1*H*-benzo[d]imidazol-6-yl)(phenyl)methanone (**12**). Recrystallized from chloroform. Yellowish white solid, yield: 70%, m.p. 195–197 °C. IR (KBr, ν cm⁻¹): 3445 (NH), 3055 (CH-aromatic), 1650 (C = O). ¹H NMR (DMSO *d*₆, 400 MHz): δ 1.91 (s, 3H, CH₃), 2.24 (s, 3H, thiazoline-CH₃), 3.93, 3.95 (2 s, 6H, 2OCH₃), 5.18 (s, 2H, N-CH₂), 6.93 (s, 1H, thiazoline-H₅), 7.01–8.59 (m, 11H, ArH), 11.5 (s, 1H, NH, D₂O exchangeable). ¹³C NMR (DMSO *d*₆, 100 MHz) δ 27.7, 29.7 (2CH₃), 56.0 (2OCH₃), 57.6 (CH₂), 112.2, 112.6, 112.9, 118.9, 122.0, 122.1, 127.8, 128.9, 129.9, 130.1, 131.7, 132.7, 146.3, 149.2, 150.9, 156.0, 196.1 (Ar-C), 203.1 (C = O). MS *m/z* (%): M⁺: 525 (90%); Anal. Calcd for: C₂₉H₂₇N₅O₃S (525.63): C, 66.27; H, 5.18; N, 13.32. Found: C, 66.27; H, 5.19; N, 13.32.

4.1.8.2. (*E*)-2-((*E*)-1-(6-benzoyl-2-(3,4-dimethoxyphenyl))-1*H*-benzo[d]imidazol-1-yl) propan-2-ylidene)hydrazineylidene)thiazolidin-4-one (**13**). Recrystallized from methanol. Gray white solid, yield: 73%, m.p. 190–192 °C. IR (KBr, ν cm⁻¹): 3437 (NH), 3055 (CH-aromatic), 1655, 1675 (2C = O). ¹H NMR (DMSO *d*₆, 400 MHz): δ 3.81 (s, 3H, CH₃), 3.93, 3.95 (2 s, 6H, 2OCH₃), 4.76 (s, 2H, thiazolidine-CH₂), 5.28 (s, 2H, N-CH₂), 7.00–7.76 (m, 11H, ArH), 11.53

(s, IH, NH, D₂O exchangeable). ¹³C NMR (DMSO *d*₆, 100 MHz) δ 26.7 (CH₃), 29.7 (thiazolidine-CH₂), 56.1 (2OCH₃), 57.6 (CH₂), 112.2, 112.6, 112.9, 118.9, 122.5, 122.1, 127.8, 128.9, 129.9, 130.1, 131.7, 132.7, 146.3, 149.2, 150.9, 156.0, 186.1 (Ar-C), 196.5, 203.1 (2C = O). MS *m/z* (%): M⁺: 527 (70%); Anal. Calcd for: C₂₈H₂₅N₅O₄S (527.60): C, 63.74; H, 4.78; N, 13.27. Found: C, 63.74; H, 4.78; N, 13.27.

4.2. Biological evaluation

4.2.1. *In vitro* anticancer activity

MTT assay was used to evaluate the *in vitro* cytotoxicity of the new compounds against Hela cell line (Thavamani et al., 2013; Prasetyaningrum et al., 2018) and WI-38 normal fibroblast cell line. MTT assay depends on the reduction of the soluble 3-(4,5-methyl-2-thiazolyl)-2,5-diphenyl-2H-tetrazolium bromide (MTT) into a blue purple formazan product, mainly by mitochondrial reductase activity inside the living cells. The cells used in cytotoxicity assay were cultured in RPMI 1640 medium supplemented with 10% fetal calf serum.

4.2.2. Kinase assays

The activities of the examined compounds against EGFR, HER2, PDGFR- β and VEGFR2 were *in vitro* tested using abcam's Human In cell ELISA Kit (ab 126419) for EGFR, ADP-Glo™ Kinase Assay for Her2, PDGFR- β , Active, Recombinant protein expressed in Sf9 cells for VEGFR2 (KDR) Kinase Assay Kit Catalog # 40325, respectively. The procedure of the used kits was done according to the manufacturer's instructions.

4.2.3. Cell cycle analysis and apoptosis detection

Cell cycle analysis and apoptosis investigation were carried out by flow cytometry (He et al., 2009; Cao et al., 2020; Yang et al., 2020). Hela cells were seeded at 8×10^4 and incubated at 37 °C, 5% CO₂ overnight. After treatment with the tested compound, for 24 h, cell pellets were collected and centrifuged (300g, 5 min).

4.2.4. Molecular docking study

The HER2 kinase domain complexed with a ligand was downloaded from the protein databank (PDB ID: 3RCD, <http://www.rcsb.org>). Protein preparation wizard of Schrödinger Suite (Sastry et al., 2013, Schrödinger, 2018) was used to correct the protein structural file by correcting bond orders, adding any missing hydrogen atoms, and completing unresolved side chains or loops. Water molecules which are beyond 5 Å of bound ligand and are not involved in at least two hydrogen bonds with non-water residues, were removed from the protein complex. The structure was then energetically minimized to remove atomic clashes. The ligand coordinates were designated as the center for docking. Glide receptor grid preparation (Friesner et al., 2006; Halgren et al., 2004; Friesner et al., 2004; Schrödinger, 2018) was used to define and construct the receptor for the docking step. To decrease penalties for close contacts between ligands and protein, 0.85 was used to scale van der Waals radii of nonpolar atoms. The hydroxyl groups of Ser, Thr, or Tyr residues in the active site were identified as rotatable groups to account for all possible hydrogen bonds with incoming ligands. Ligand structures were prepared

by LigPrep (Schrödinger, 2018). Standard-precision (SP) docking option was chosen for the docking experiment, and Glide was directed to generate ligand conformations through the docking process.

Funding

This research did not receive any specific grant from funding agencies in the public, commercial, or not-for-profit sectors.

Declaration of Competing Interest

The authors declared that there is no conflict of interest.

Appendix A. Supplementary data

Supplementary data to this article can be found online at <https://doi.org/10.1016/j.arabjc.2020.10.041>.

References

- Abbas, H.-A., Abd El-Karim, S.S., 2019. Design, synthesis and anticervical cancer activity of new benzofuran-pyrazol-hydrazono-thiazolidin-4-one hybrids as potential EGFR inhibitors and apoptosis inducing agents. *Bioorg. Chem.* 89, 103035. <https://doi.org/10.1016/j.bioorg.2019.103035>.
- Abd El-Meguid, E.A., Awad, H.M., Anwar, M.M., 2019. Synthesis of New 1,3,4-Oxadiazole-benzimidazole Derivatives as Potential Antioxidants and Breast Cancer Inhibitors with Apoptosis Inducing Activity. *Russ. J. Gen. Chem.* 89 (2), 348–356.
- El-Meguid, E.A.A., Ali, M.M., 2016. Synthesis of some novel 4-benzothiazol-2-yl-benzoyl-1H-pyrazoles, and evaluation as antiangiogenic agents. *Res. Chem. Intermed.* 42 (2), 1521–1536.
- Cao, Y.i., Xiong, J.-B., Zhang, G.-Y., Liu, Y.i., Jie, Z.-G., Li, Z.-R., 2020. Long Noncoding RNA UCA1 Regulates PRL-3 Expression by Sponging MicroRNA-495 to Promote the Progression of Gastric Cancer. *Mol. Ther. Nucleic Acids* 19, 853–864.
- Das, D., Xie, L., Wang, J., Xu, X., Zhang, Z., Shi, J., Le, X., Hong, J., 2019. Discovery of new quinazoline derivatives as irreversible dual EGFR/HER2 inhibitors and their anticancer activities – Part 1. *Bioorg. Med. Chem. Lett.* 29 (4), 591–596.
- El-Sherief, H.A.M., Youssif, B.G.M., Abbas Bukhari, S.N., Abdelazeem, A.H., Abdel-Aziz, M., Abdel-Rahman, H.M., 2018. Synthesis, anticancer activity and molecular modeling studies of 1,2,4-triazole derivatives as EGFR inhibitors. *Eur. J. Med. Chem.* 156, 774–789.
- Elzahhar, P.A., Alaaeddine, R., Ibrahim, T.M., Nassra, R., Ismail, A., Chua, B.S.K., Frkic, R.L., Bruning, J.B., Wallner, N., Knape, T., von Knethen, A., Labib, H., El-Yazbi, A.F., Belal, A.S.F., 2019. Shooting three inflammatory targets with a single bullet: Novel multi-targeting anti-inflammatory glitazones. *Eur. J. Med. Chem.* 167, 562–582.
- Friesner, R.A., Banks, J.L., Murphy, R.B., Halgren, T.A., et al, 2004. Glide: A New Approach for Rapid, Accurate Docking and Scoring. 1. Method and Assessment of Docking Accuracy. *J. Med. Chem.* 47, 1739–1749. <https://doi.org/10.1021/jm0306430>.
- Friesner, R.A., Murphy, R.B., Repasky, M.P., et al, 2006. Extra precision glide: docking and scoring incorporating a model of hydrophobic enclosure for protein-ligand complexes. *J. Med. Chem.* 49 (21), 6177–6196. <https://doi.org/10.1021/jm051256o>.
- Goncalves, A., Fabbro, M., Lhommé, C., Gladieff, L., Extra, J.-M., Floquet, A., Chaigneau, L., Carrasco, A.T., Viens, P., 2008. A phase II trial to evaluate gefitinib as second- or third-line treatment

- in patients with recurring locoregionally advanced or metastatic cervical cancer. *Gynecol. Oncol.* 108 (1), 42–46.
- Halgren, T.A., Murphy, R.B., Friesner, R.A., et al, 2004. Glide: a new approach for rapid, accurate docking and scoring. 2. Enrichment factors in database screening. *J. Med. Chem.* 47(7):1750–1759. <https://doi.org/10.1021/jm030644s>.
- He, B., Lu, N., Zhou, Z., 2009. Cellular and nuclear degradation during apoptosis. *Curr. Opin. Cell Biol.* 21 (6), 900–912.
- Hou, W., Sun, H., Ma, Y., Liu, C., Zhang, Z., 2019. Identification and Optimization of Novel Cathepsin C Inhibitors Derived from EGFR Inhibitors. *J. Med. Chem.* 62 (12), 5901–5919.
- Akhtar, M.J., Khan, A.A., Ali, Z., Dewangan, R.P., Rafi, M.d., Hassan, M.Q., Akhtar, M.S., Siddiqui, A.A., Partap, S., Pasha, S., Yar, M.S., 2018. Synthesis of stable benzimidazole derivatives bearing pyrazole as anticancer and EGFR receptor inhibitors. *Bioorg. Chem.* 78, 158–169.
- Knight, Z.A., Lin, H., Shokat, K.M., 2010. Targeting the cancer kinase through polypharmacology. *Nat. Rev. Cancer* 10 (2), 130–137.
- Kujtan, L., Subramanian, J., 2019. Epidermal growth factor receptor tyrosine kinase inhibitors for the treatment of non-small cell lung cancer. *Expert Rev. Anticancer Ther.* 19 (7), 547–559.
- Li, Y., Tan, C., Gao, C., Zhang, C., Luan, X., Chen, X., Liu, H., Chen, Y., Jiang, Y., 2011. Discovery of benzimidazole derivatives as novel multi-target EGFR, VEGFR-2 and PDGFR kinase inhibitors. *Bioorg. Med. Chem.* 19 (15), 4529–4535.
- Oh, D.-Y., Kim, S., Choi, Y.-L., Cho, Y.J., Oh, E., Choi, J.-J., Jung, K., Song, J.-Y., Ahn, S.E., Kim, B.-G., Bae, D.-S., Park, W.-Y., Lee, J.-W., Song, S., 2015. HER2 as a novel therapeutic target for cervical cancer. *Oncotarget* 6 (34), 36219–36230.
- Pérez-Regadera, J., Sánchez-Muñoz, A., De-la-Cruz, J., Ballestín, C., Lora, D., García-Martín, R., Sotoca, A., Pérez-Ruiz, E., Lanzós, E., 2011. Impact of Epidermal Growth Factor Receptor Expression on Disease-Free Survival and Rate of Pelvic Relapse in Patients With Advanced Cancer of the Cervix Treated With Chemoradiotherapy. *Am. J. Clin. Oncol.* 34 (4), 395–400.
- Prasetyaningrum, P.W., ID, A.B., Hayun, H., 2018. Synthesis and Cytotoxicity Evaluation of Novel Asymmetrical Mono-Carbonyl Analogs of Curcumin (AMACs) against Vero, HeLa, and MCF7 Cell Lines. *Sci. Pharm.*, 86, 25; doi:10.3390/scipharm86020025.
- Šarenac, T. and Mikov, M., 2019. Cervical Cancer, Different Treatments and Importance of Bile Acids as Therapeutic Agents in This Disease, *Frontiers in Pharmacology* 10 Article 484. <https://doi.org/10.3389/fphar.2019.00484>.
- Madhavi Sastry, G., Adzhigirey, M., Day, T., Annabhimoju, R., Sherman, W., 2013. Protein and ligand preparation: parameters, protocols, and influence on virtual screening enrichments. *J. Comput Aided Mol Des* 27 (3), 221–234.
- Schilder, R.J., Sill, M.W., Lee, Y.-C., Mannel, R., 2009. A Phase II Trial of Erlotinib in Recurrent Squamous Cell Carcinoma of the Cervix: A Gynecologic Oncology Group Study. *Int. J. Gynecological Cancer* 19 (5), 929–933.
- Schrödinger Release 2018-4: Protein Preparation Wizard; Epik, Schrödinger, LLC, New York, NY, 2016; Impact, Schrödinger, LLC, New York, NY, 2016; Prime, Schrödinger, LLC, New York, NY, 2018.
- Schrödinger Release 2018-4: Glide, Schrödinger, LLC, New York, NY, 2018.
- Schrödinger Release 2018-4: LigPrep, Schrödinger, LLC, New York, NY, 2018.
- Sharma, Prabodh Chander, Bansal, Kushal Kumar, Sharma, Archana, Sharma, Diksha, Deep, Aakash, 2020. Thiazole-containing compounds as therapeutic targets for cancer therapy. *Eur. J. Med. Chem.* 188, 112016. <https://doi.org/10.1016/j.ejmech.2019.112016>.
- Shrivastava, Neelima, Naim, Mohd. Javed, Alam, Md. Jahangir, Nawaz, Farah, Ahmed, Shujauddin, Alam, Ozair, 2017. Benzimidazole Scaffold as Anticancer Agent: Synthetic Approaches and Structure-Activity Relationship: Benzimidazole Scaffold as Anticancer Agent. *Arch. Pharm. Chem. Life Sci.* 350 (6), e201700040. <https://doi.org/10.1002/ardp.v350.610.1002/ardp.201700040>.
- Smolobochkin, A., Gazizov, Almir, Sazykina, M. et al., 2019. Synthesis of Novel 2-(Het)arylpyrrolidine Derivatives and Evaluation of Their Anticancer and Anti-Biofilm Activity. *Molecules.* 24 (17), 3086. doi: 10.3390/molecules24173086.
- Soliman, Aiten M., Alqahtani, Ali S., Ghorab, Mostafa M., 2019. Novel sulfonamide benzoquinazolinones as dual EGFR/HER2 inhibitors, apoptosis inducers and radiosensitizers. *J. Enzyme Inhib. Med. Chem.* 34 (1), 1030–1040.
- Thavamani, B.S., Mathew, M., Dhanabal, S.P., 2013. In vitro cytotoxic activity of menispermaceae plants against HeLa cell line. *Ancient Sci. life* 33 (2), 81–84. <https://doi.org/10.4103/0257-7941.139040>.
- Ueda, A., Takasawa, A., Akimoto, T. et al., 2017. Prognostic significance of the co-expression of EGFR and HER2 in adenocarcinoma of the uterine cervix, *PLoS ONE* 12(8) e0184123. <https://doi.org/10.1371/journal.pone.0184123>.
- Vora, Chakor, Gupta, Sudeep, 2018. Targeted therapy in cervical cancer. *ESMO Open* 3 (Suppl 1), e000462. <https://doi.org/10.1136/esmoopen-2018-000462>.
- Wang, Caolin, Xu, Shan, Peng, Liang, Zhang, Bingliang, Zhang, Hong, Hu, Yingying, Zheng, Pengwu, Zhu, Wufu, 2019. Design, synthesis and biological evaluation of novel 4-anilinoquinazoline derivatives as EGFR inhibitors with the potential to inhibit the gefitinib-resistant nonsmall cell lung cancers. *J. Enzyme Inhib. Med. Chem.* 34 (1), 203–217.
- Yang, Chao, Yan, Zeqiang, Hu, Fen, Wei, Wei, Sun, Zhihua, Xu, Wei, 2020. Silencing of microRNA-517a induces oxidative stress injury in melanoma cells via inactivation of the JNK signaling pathway by upregulating CDKN1C. *Cancer Cell Int* 20 (1). <https://doi.org/10.1186/s12935-019-1064-y>.
- Zhang, H., 2016. Osimertinib making a breakthrough in lung cancer targeted therapy. *OncoTargets and Therapy* 9, 5489–5493. <https://doi.org/10.2147/OTT.S114722>.
- Zou, Min, Jin, Bo, Liu, Yanrong, Chen, Huiping, Zhang, Zhuangli, Zhang, Changzheng, Zhao, Zhihong, Zheng, Liyun, 2018. Synthesis and Biological Evaluation of Some Novel Thiophene-bearing Quinazoline Derivatives as EGFR Inhibitors. *LDDD* 16 (2), 102–110.